LAUR-92-500

MODELLING SURFACE MOTION AND SPALL AT THE NEVADA TEST SITE

Fred N. App
Wendee M. Brunish
EES-3

Los Alamos Source Region Project

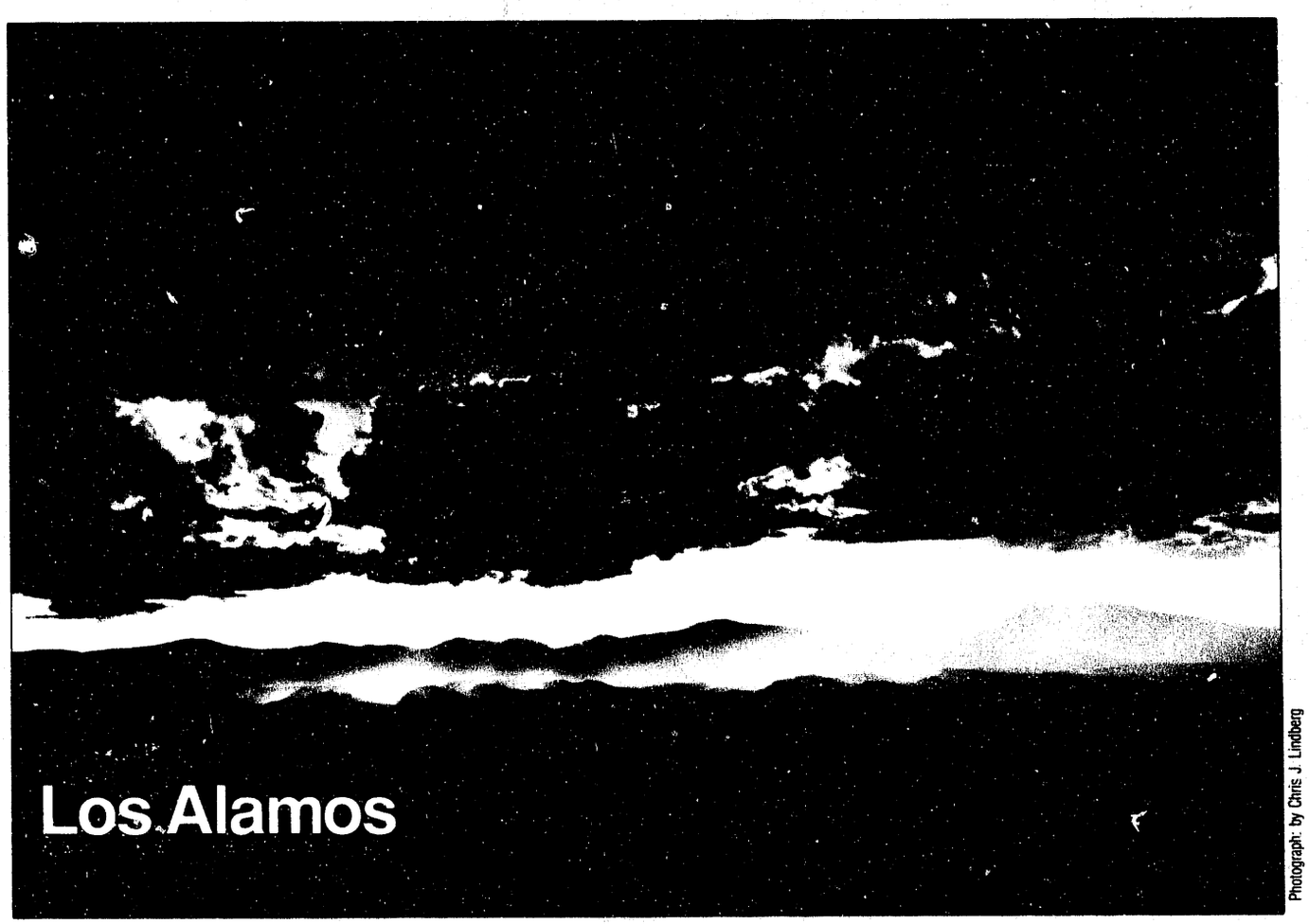

Photograph: by Chris J. Lindberg

Modelling Surface Motion and Spall at the Nevada Test Site

Fred N. App
Wendee M. Brunish

Los Alamos National Laboratory

January 1992

CONTENTS

Modeling Surface Motion and Spall at the Nevada Test Site

by
Fred N. App and Wendee M. Brunish
Los Alamos National Laboratory

Abstract

Spallation of the ground surface accompanies all underground nuclear explosions of significant yield. We use computer modelling to investigate the physical processes that govern spallation and the amplitude and wavelength of motion at the free surface under a variety of conditions. Four events are selected: MERLIN which was conducted in desert alluvium; HEARTS which was conducted in tuff beneath the water table in Yucca Flat; TOWANDA which was conducted beneath the water table on Pahute Mesa; and HOUSTON which was conducted above the water table in very dense rock on Pahute Mesa. These span the range of test environments for Los Alamos underground nuclear tests. As a result of these investigations, we are able to offer a plausible explanation for the less than negative 1 g "spall" accelerations so often observed on low yield events conducted in alluvium. We believe it is associated with near surface shear failure of the alluvium as the incident wave is reflected at the free surface. For "HEARTS class" events, the phenomena of "delayed spall" at surface ground zero (SGZ) and the transition to more "N shaped" velocity waveforms away from SGZ appear to be strong functions of the thickness of the alluvium and the WP properties. Peak motions away from SGZ are less sensitive to details of the geology than are those near SGZ. There are three distinct "pulses" that determine the amplitude and period of motion at SGZ: 1) the elastic precursor, 2) the remnant of the plastic wave and 3) a pulse generated by an elastic "rebound" at depth. Spallation on Pahute Mesa appears to be less complicated than in Yucca Flat due to the lack of alluvium at the surface. For TOWANDA and HOUSTON, we determine that the WP saturation and strength of the rocks out to a few cavity radii are primarily responsible for the observed amplitude differences in surface motions between those two events. At TOWANDA, a near surface low velocity layer appears to have considerable influence on spall depth. The calculations indicate that for the events not conducted in alluvium, the kinetic energy associated with spall, and potentially available as a secondary source of seismic waves, is about one-fourth that available for seismic waves radiating out from the point source explosion.

I. INTRODUCTION

The factors influencing surface motion and spall attending underground nuclear explosions has been the subject of numerous studies and papers over the years. Rinehart (1960) dealt with the mechanics of the spall process and the creation of slabs (in the case of rock) and "flakes" (in incompetent material such as alluvium) during the spall process. The work of Eisler and Chilton (1964), Chilton, Eisler and Heubach (1966) and Eisler, Chilton and Sauer (1966) progressed through investigations of spall in tuff, halite and alluvium. It was determined that processes in alluvium were of a different nature than those in the halite and tuff. Perret (1971) studied and reported on all aspects of stress wave related phenomenology for the MERLIN alluvium event, including surface motion and spall. This work is of particular interest to us since MERLIN is one of the subject events of our current work. Glenn (1976) used the SOC one-dimensional finite difference stress wave code in analyzing spall in one-dimension (spherical symmetry). He looked at the influence of material properties on surface motion and spall.

More recent work that is of special interest to us is that of Patton (1990) and Stump and Weaver (1991). These works are directed toward development of a spall source model for the Arms Control and Treaty Verification programs. Stump and Weaver propose a spall source model that couples free-field attenuation with free surface reflection. Patton has analyzed over 30 Pahute Mesa events for characterization of the spall source and has developed an algorithm for estimating the mass and energy associated with spall. An event he was able to analyze in detail, owing to the availability of high quality data in the spall region, was TOWANDA which also is one of the subject events of our study.

Our interest lies not only with arms control verification but also with the containment of underground nuclear tests. The relevance of surface motion to containment has never been firmly established, but the feeling of many in the containment community is that conditions that lead to exceptionally strong ground motion are to be avoided. We feel that the best, and perhaps the only way, to establish relevancy is through the use of stress wave calculations that model all the physical processes from inception of the explosion through spall and spall closure.

In this paper we present the results of calculations in support of both the Los Alamos Nuclear Containment Program and the Arms Control and Treaty Verification Program. It is not within the scope of the current phase of the study to fold results in with the work of Stump and Weaver (1991), Patton (1990) or others, but that certainly is our intent in the very near future. The emphasis of this paper is in evaluating our ability to model the important aspects of spall, to develop additional understanding of the underlying physical

processes involved and to look at the influence of various shot configurations and geologic circumstances on surface motion and spall. For both containment and verification applications, an obvious advantage to using a modelling approach is that the analysis can be extended to situations that are not covered by experience and are not amenable to experiment. The obvious difficulty is in assuring that we are capturing the relevant physical processes with response models that necessarily are a gross simplification and approximation of the true nature of things.

II. APPROACH

MERLIN, HEARTS, TOWANDA and HOUSTON are representative of Los Alamos tests conducted in a) dry alluvium, b) moderate density tuff overlain by alluvium, c) moderate density tuff with no alluvial cover and d) dense tuff and lava with no alluvial cover, respectively. These span the range of environments for Los Alamos underground nuclear tests. For each of the four tests, subsurface ground motion measurements are available to provide a picture of how the explosion generated stress wave evolves as it propagates toward and reflects from the ground surface. To complete the picture, there are free surface motion measurements to greater than one depth-of-burial (DOB) horizontal range from surface ground zero (SGZ).

By forward, iterative computer modelling and waveform matching of the subsurface motion data, we are able to infer many of the in-situ response properties of the rocks at each of the four event sites. This approach is indicated because of the extreme difficulty encountered in obtaining such properties from laboratory tests on core, particularly for materials lacking cohesiveness and/or containing large inclusions such as alluvium or for rock masses containing numerous macro-scale fractures such as Pahute Mesa tuffs and lavas. For MERLIN and HEARTS, we build on our previous modelling efforts (Brunish and App, 1989; App, Brunish and Edwards, 1989; App and Brunish, 1991). The HOUSTON/TOWANDA work is new and is not as complete.

In this study, the emphasis is on surface motion and spall and we address only those aspects of the calculations directly relevant to this issue. Our approach is to use the best calculation (i.e., the most realistic inferred response properties and best waveform matches) for each of the four events as a "Baseline Case" and use it in analyzing the physical processes involved in spall. Then we perform a limited set of parameter/sensitivity studies varying event and site parameters such as yield, DOB, mechanical properties and layering to demonstrate the influence of such changes on surface motion and spall. In this paper, we report on the Baseline Case for each of the four events but limit the reporting on parameter studies to just MERLIN and HEARTS. We place emphasis on the physical

processes inferred from the studies and limit discussion on the details of the response models employed and how we developed them. Some of the model development was covered in our earlier reports.

For stress wave calculations, we use a Los Alamos modified version of the Sandia National Laboratory TOODY finite difference stress wave code (Swegle, 1978). All calculations are run in a two-dimensional mode with cylindrical symmetry about a vertical axis. By locating the energy source on the axis of symmetry we achieve the necessary spherical divergence for stress wave propagation. In most cases, two-dimensions limits us to representing the geology at each site as having horizontal layering with no lateral changes in properties, although bedding dip or lateral variations can be modelled if one can tolerate the distortions caused by the cylindrical geometry. For the purposes of this study, the assumption of horizontal layering is not a serious limitation. We employ a rectangular computational mesh with rectangular zones a few meters on a side in the region near the axis of symmetry and from the working point (WP) to the surface, grading to larger size zones away from the regions of interest. The mesh is preset with hydrostatic overburden pressure and the acceleration of gravity is set to 9.8 m/s^2. Air above the ground surface is not included in the calculations but there is no computational limitation precluding this. The ground surface is modelled as a free boundary. A calculation is initiated by depositing the appropriate amount of energy into a few zones followed by frequent rezoning to disentangle the mesh during rock vaporization and cavity expansion. For this study, an appropriate treatment for tensile failure is important. For each computational zone and for each step in time, the stress tensor is rotated into its principle stress components and tested against a tensile failure criteria (tensile strength). If the criteria is met, that particular component of stress is relaxed to zero and the tensile strength for the zone is set to zero. The mesh does not physically separate during tensile failure, rather failed zones expand and become rarefied at zero stress. For the selection of calculations presented here, we use zero as the tensile strength for all geologic materials. This is on the basis of general field observations of naturally occurring fractures in tuffs and lavas or, in the case of alluvium, the observed lack of cohesiveness. Additional details on the constitutive models used in our version of the TOODY code are available in Apn and Brunish (1991).

III. RESULTS

MERLIN - A Low Yield Event Conducted in Alluvium.

Figure 1 shows the subsurface and surface motion station locations for MERLIN. The 10 kt event was conducted above the water table in desert alluvium at a depth of 296 m and a scaled-depth-of-burial (SDOB) of 137 m/kt1/3. In our previous MERLIN work (Brunish and App, 1989), we established that the alluvium at the MERLIN site can be loaded up to 1.2 MPa stress before significant pore crush occurs, thus leading to the development of a distinctive elastic precursor in the propagating stress wave. We also established that the material is exceptionally weak in shear with an unconfined strength of nearly zero. In the MERLIN Baseline Case, the properties of the alluvium are the same at all depths with the following exceptions: 1) the surface layer down to 28 m is modelled as a uniform, low velocity (weathered) layer that is even weaker in shear than the already very weak deeper material and 2) below 28 m the velocity gradually increases with depth in a manner consistent with the measurements. The motion data was collected and first analyzed by Sandia National Laboratory (Perret, 1971). Figure 2 shows the calculated and measured vertical particle velocity waveforms to a depth of 92 m. The measurements are hand digitized from figures in the MERLIN report (Perret, 1971). The calculated risetimes and peak amplitudes agree well with the measurements. Later phases are not in as close agreement. The calculated stress wave for MERLIN at these same locations (Figure 3) is a very broad, low amplitude pulse. Spall, as defined by the zero stress condition, is erratic and of short duration. The stress wave for an event conducted in competent rock at the same yield and DOB would have a much shorter risetime, higher amplitude and a longer spall duration than shown here.

Figure 4 shows free surface vertical and horizontal particle velocity waveforms at Station S2, which is near SGZ, and Station S8, which is located 454 m away from SGZ and is well outside the MERLIN spall region. At S2, the calculated waveform is not quite as broad as the measurement but the main features such as the initial rise, the peak amplitude, spall duration and recompaction (slapdown) are captured. At Station S8, the calculation reproduces the initial upward motion reasonably well and there is no spallation. There is poorer agreement between the measured and calculated horizontal components. The calculation leads the measurement by almost 100 ms indicating the presence of lateral variations in sound speed at the MERLIN site (that are not modelled). Also, from a tangential measurement at S8 (not shown), there is a suggestion that three-dimensional effects have become significant by about 800 ms.

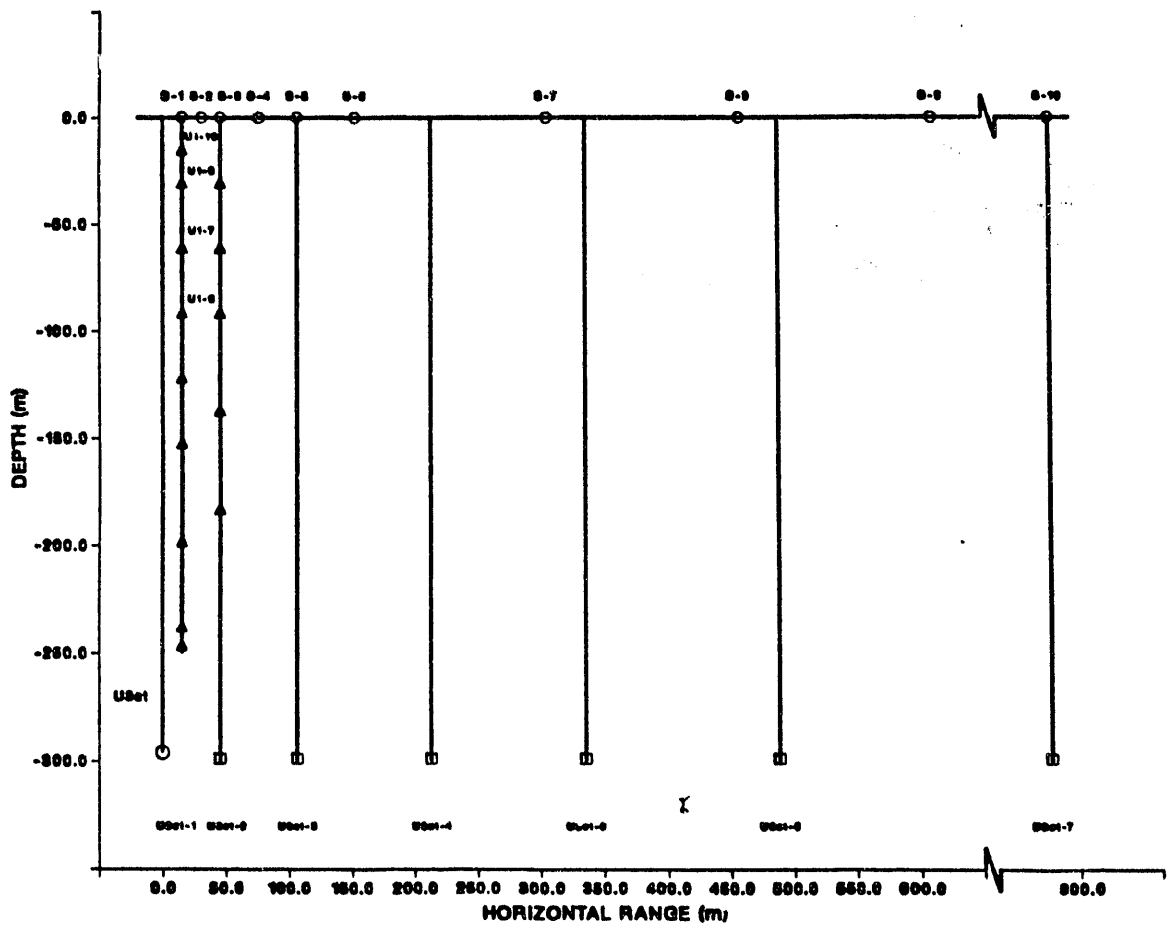

Figure 1. MERLIN ground motion station locations. Triangles represent vertical accelerometer stations, squares represent horizontal accelerometer stations at WP level, circles represent three component surface accelerometer stations. Material is alluvium.

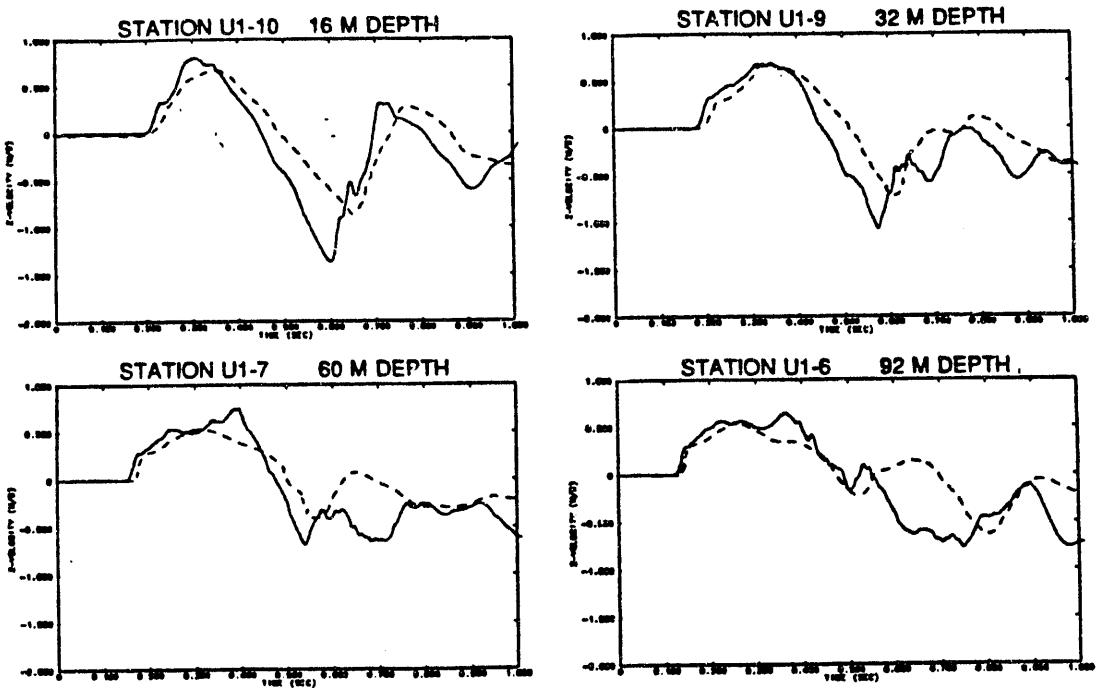

Figure 2. Comparison of calculated (solid) vs measured (dashed) particle velocity waveforms from 16 to 92 m depth. MERLIN Baseline Case.

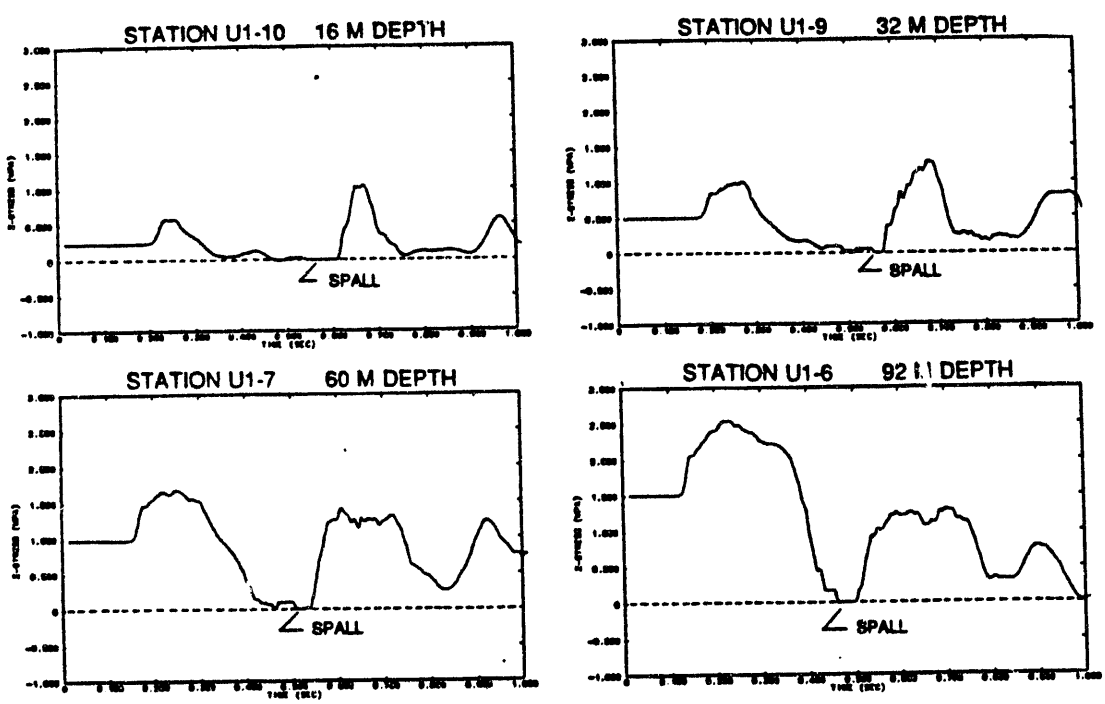

Figure 3. Calculated vertical stress waveforms from 16 to 92 m depth. Zero stress denotes spall. MERLIN Baseline Case.

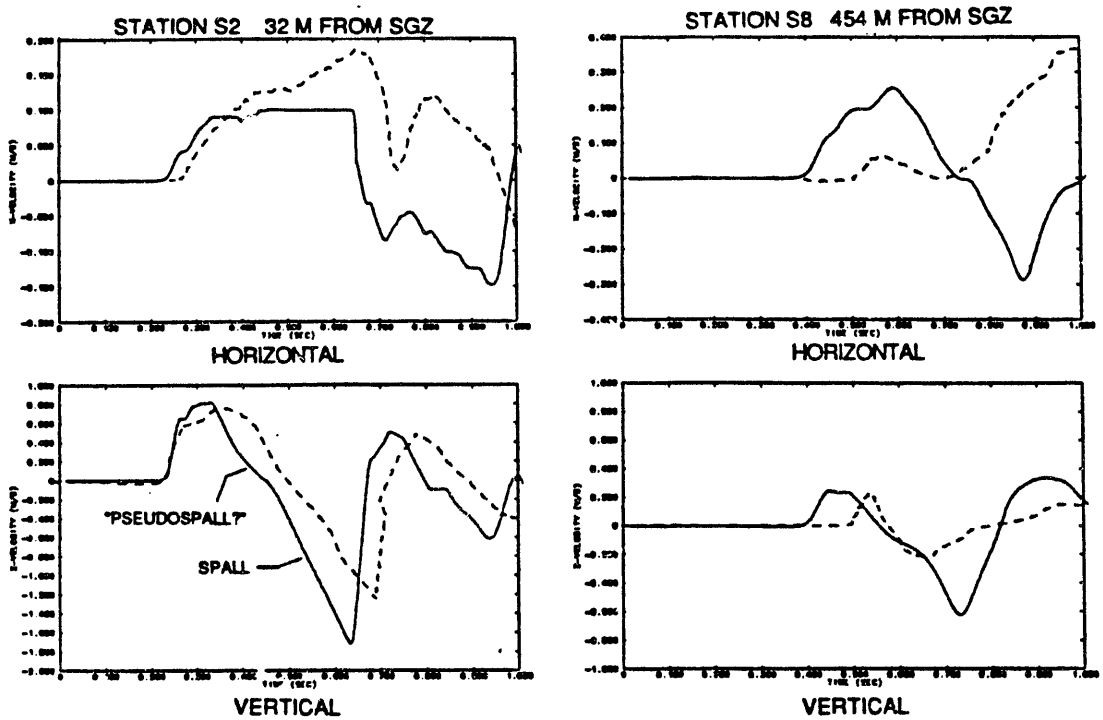

Figure 4. Comparison of calculated (solid) vs measured (dashed) horizontal and vertical free surface velocity waveforms at Stations S2 and S8. MERLIN Baseline Case.

An interesting aspect of low yield events conducted in alluvium is the less than 1 g downward "spall" acceleration observed at the free surface. Perret (1971) in his analysis of the MERLIN data sometimes referred to it as "pseudospallation". Significantly, the calculations also exhibit some "pseudospallation", but to a lesser extent than measured.

Inasmuch as the calculations are replicating much of the observed behavior, they can be used to analyze the physical processes involved in spall and "pseudospall" in alluvium. Figure 5 is a series of time "snapshots" of zero pressure contours that show spallation (hatched areas) as it develops in the calculation. During the early stages of spall (420 and 480 ms), partings are erratic and discontinuous. In the calculation, the incident stress wave is elastic; but when it is reflected at the free surface as a rarefaction, the near surface alluvium becomes less confined and begins failing in shear (recall the almost zero unconfined strength), which in turn inhibits tensile failure. Figure 6 illustrates this process. Shown are the calculated vertical acceleration, particle velocity and stress at an edit point located 8 m beneath Station S6 at 152 m surface range. The measured and calculated motion at the surface also are shown. At 8 m depth and during the time interval from 340 ms to 500 ms, the alluvium unloads but does not spall. Instead the material enters a shear failure mode which broadens the wave and delays spall. Unlike the measurement, calculated spall finally does occur at 500 ms. Figure 7 is similar to Figure 6 but for Station S8 at 454 m range. Here, the material never does spall in the calculation but there still is present what could be interpreted as a "pseudospall" closure. Again, the near surface material fails in shear as it unloads during the surface reflection. A point to be made is that the reflected stress profile is not the mirror image of the incident wave, contrary to what usually is assumed in classical spall analyses. Therefore, the depth and duration of spall cannot be predicted on the basis of an incident wave's period and amplitude alone. Also, as suggested in Figure 7, a measurement at the surface can show many of the characteristics of spall such as a spall closure phase, without the near surface alluvium actually being separated from the material beneath it. Shear failure during reflection of the low amplitude, broad incident wave, perhaps in combination with some very minor, discontinuous and short lived tensile failure, is what we believe is responsible for "pseudospallation" in alluvium.

Recognizing that the calculation appears to overestimate spall, it still is of interest to note the energy partitioning between spalled and unspalled material. In relating it to MERLIN, perhaps we can consider it as energy partitioning between understressed, nearly spalled material and "normal" (near overburden) stress material. At the peak of spall at 580 ms, the total kinetic energy within the calculated spall region is 3.6 GJ (~0.9 tonnes). This represents about 0.009 percent of the total explosive energy of the MERLIN device. On the other hand, the total kinetic energy in the elastic field outside the damaged regions, and

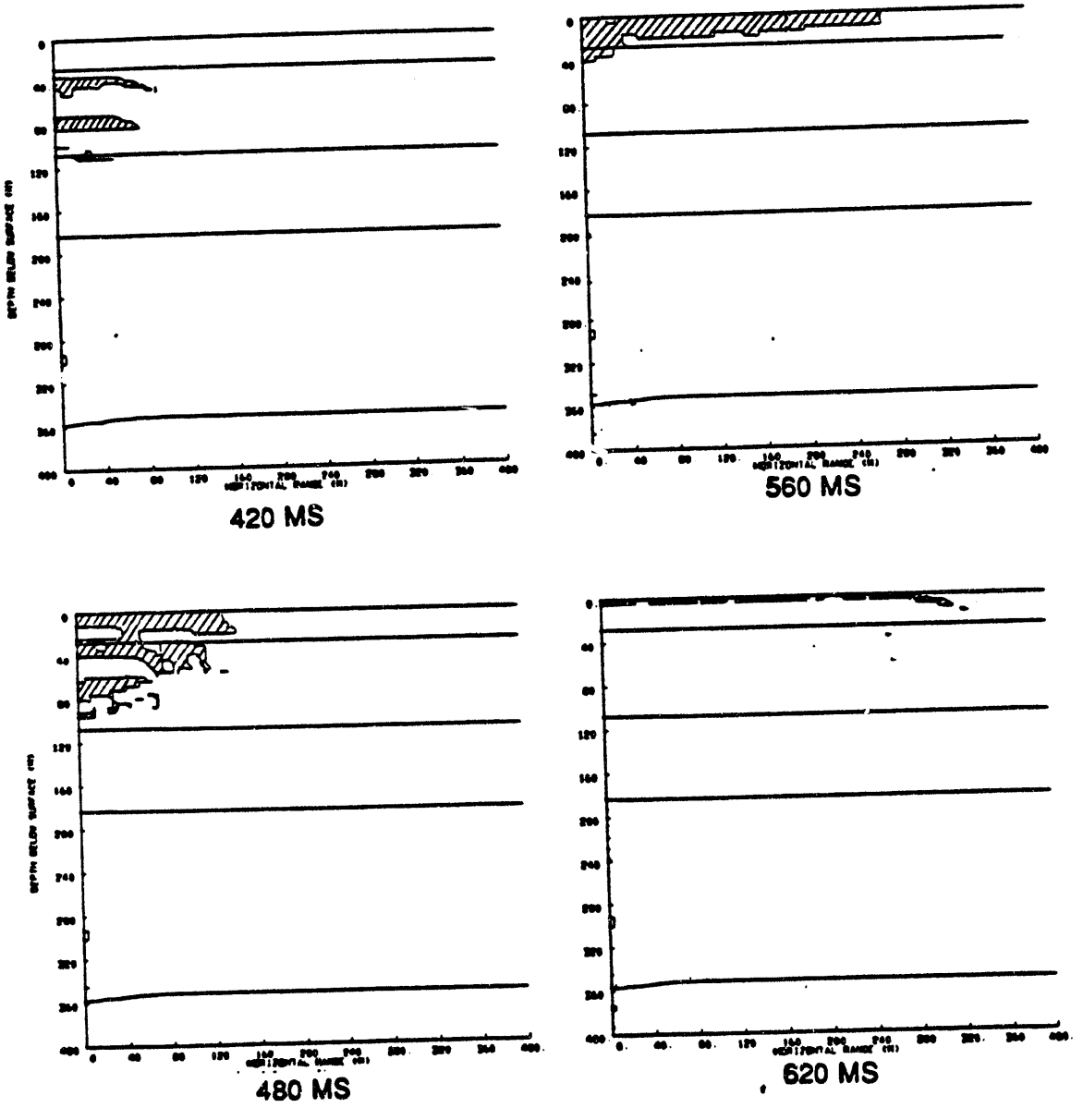

Figure 5. Evolution of spall from 420 to 620 ms. MERLIN Baseline Case. Regions of zero stress (spall) are hatched.

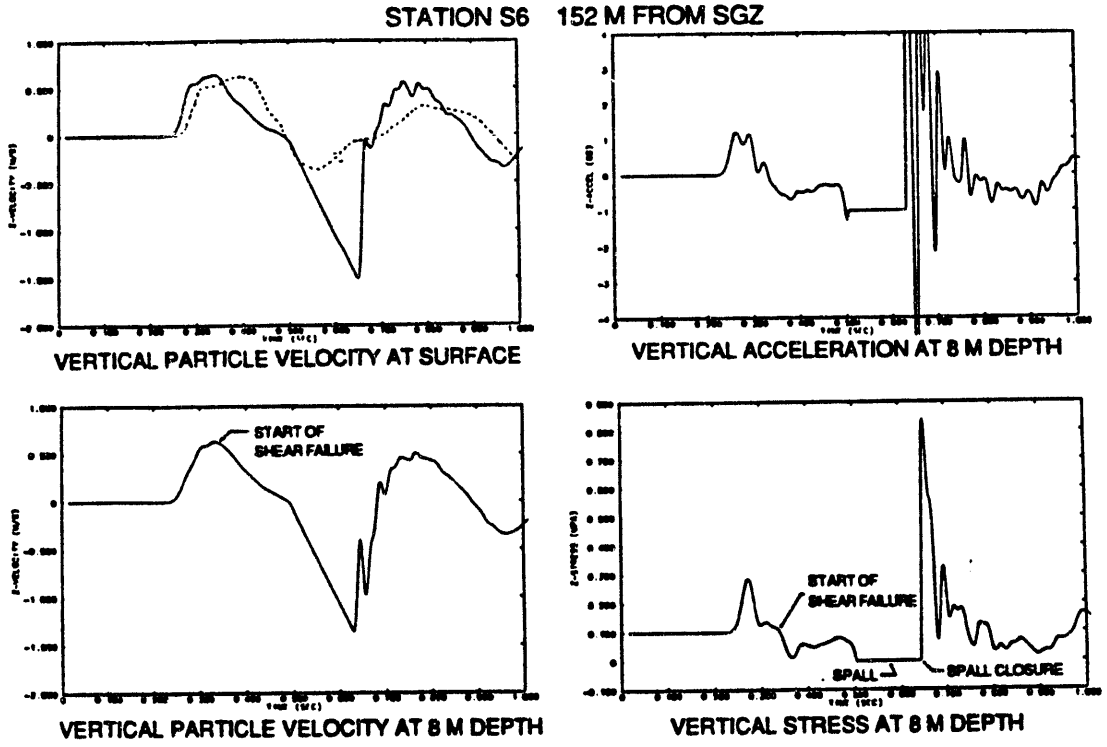

Figure 6. Calculated acceleration, velocity and stress waveforms from 8 m below Station S6 showing processes involved in spall and "pseudospall". Also shows calculated (solid) vs measured (dashed) vertical particle velocity at surface. MERLIN Baseline Case.

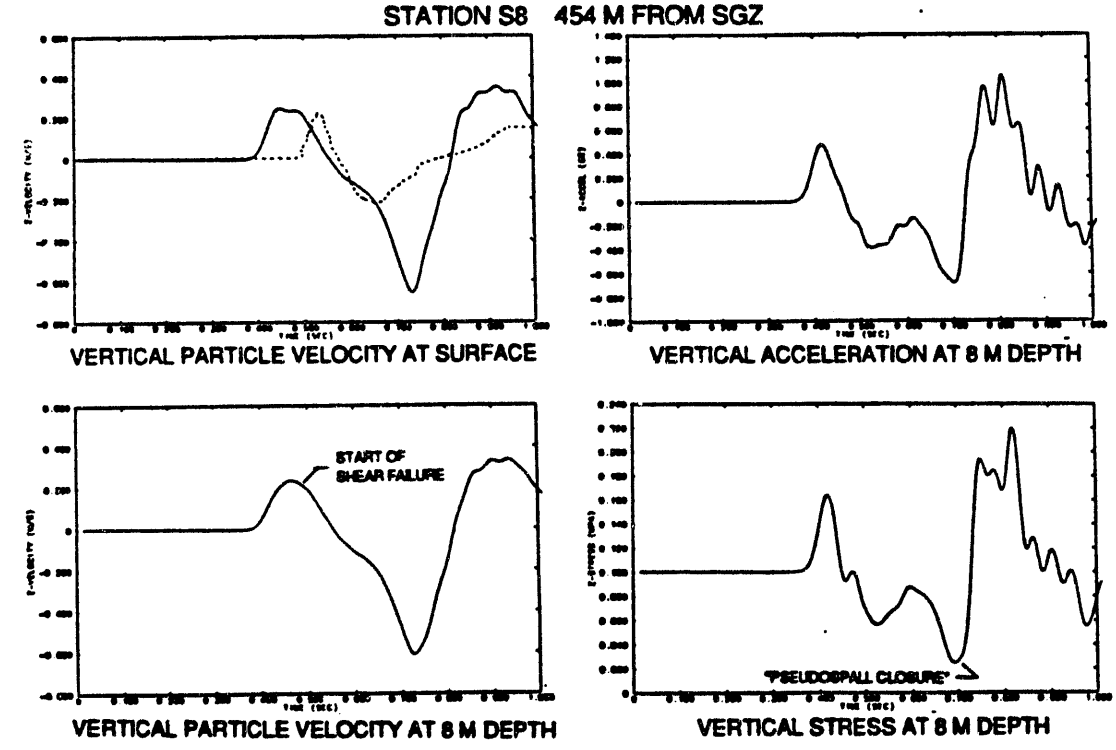

Figure 7. Calculated acceleration, velocity and stress waveforms from 8 m below Station S8 showing processes involved in "pseudospall". Also shows calculated (solid) vs measured (dashed) vertical particle velocity at surface. MERLIN Baseline Case.

presumably in the form of seismic waves, is about 35 GJ (~8.4 tonnes - 0.08 percent of the MERLIN yield). For seismic source region considerations, the energy potentially available for generation of seismic signals during spall closure is about one-tenth of that potentially available for seismic waves radiating from the point source explosion.

We have some words of caution regarding the energy in the elastic field. A slight equilibrium imbalance in the computational mesh causes some conversion between potential energy (i.e., overburden stress) and internal and kinetic energy, confusing the picture somewhat as to how much of the kinetic energy actually is associated with outward propagating elastic waves. The error associated with this increases exponentially with time and is small if we edit for elastic field energy relatively early in the problem. We decided to choose a peak value of "elastic" kinetic energy which occurs about midway through a typical calculation, recognizing that there may still be a small amount of material in the problem that has yet to fail. This derived value for elastic kinetic energy probably is an upper bound. We also are making the assumption that all energy that does not go into rock vaporization, melt, crush, inelastic shear deformation or tensile failure is available for seismic wave generation, and is the only energy so available. Having said all this, we note that the calculated value of .08 percent of energy potentially available for seismic wave generation is in good agreement with Perret's (1971) estimate of 0.04 percent that he derived by integrating the MERLIN shot level station waveforms for energy, and assuming spherical symmetry. We plan further work specifically to look into possible sources of error in our elastic energy edits and to test our assumptions regarding energy actually associated with seismic wave propagation. The above cautions apply to all elastic field energy edits discussed in this paper.

MERLIN Parameter Studies

Case A - Higher Strength Alluvium. In our analysis of MERLIN, we emphasized the effect of material strength on spall phenomenology. Here we somewhat arbitrarily increase the strength of the alluvium by 50 percent. To achieve this, we a) increase the crush threshold pressure from 1.2 to 1.8 MPa, b) increase the pressure at which pore crush is complete from 30 Mpa to 45 Mpa and c) increase the shear strength at any given confining pressure by 50 percent.

Figure 8 shows the calculated and measured particle velocity waveforms to a depth of 92 m. Comparing this to Figure 2, we observe that peak amplitudes are about 50 percent higher and spall is stronger to a depth of 32 m. Figure 9 shows vertical and horizontal particle velocity waveforms at the free surface (to be compared with Figure 4). There is less "pseudospallation" and a stronger negative 1 g component in the calculation with increased strength alluvium.

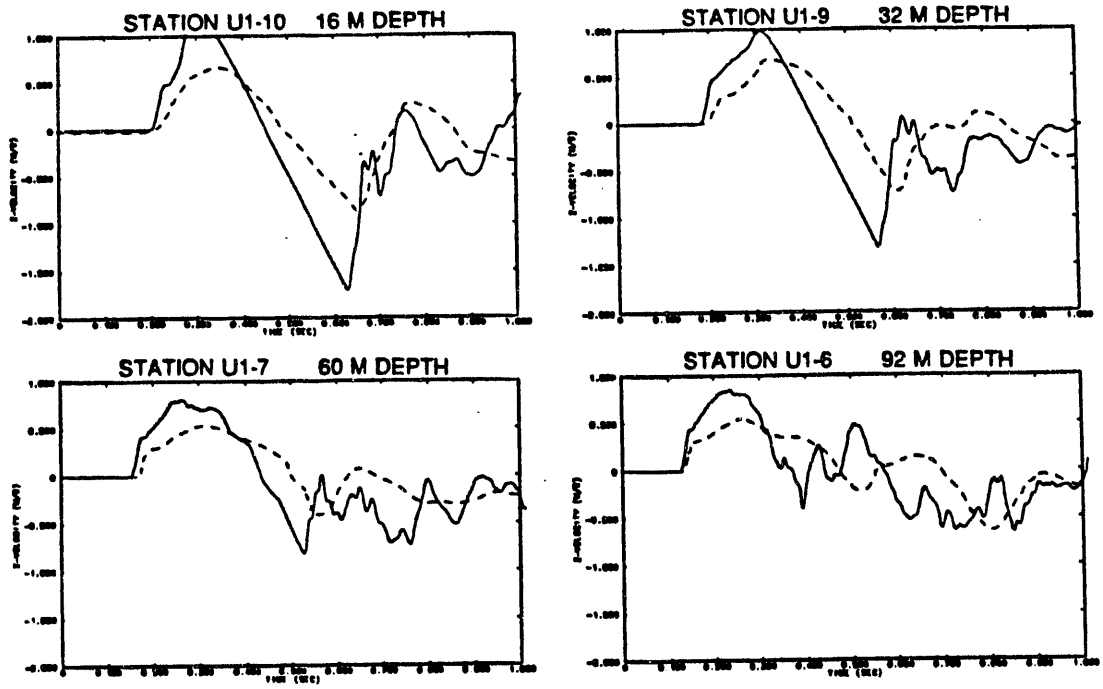

Figure 8. Comparison of calculated (solid) vs measured (dashed) particle velocity waveforms from 16 to 92 m depth. MERLIN Case A.

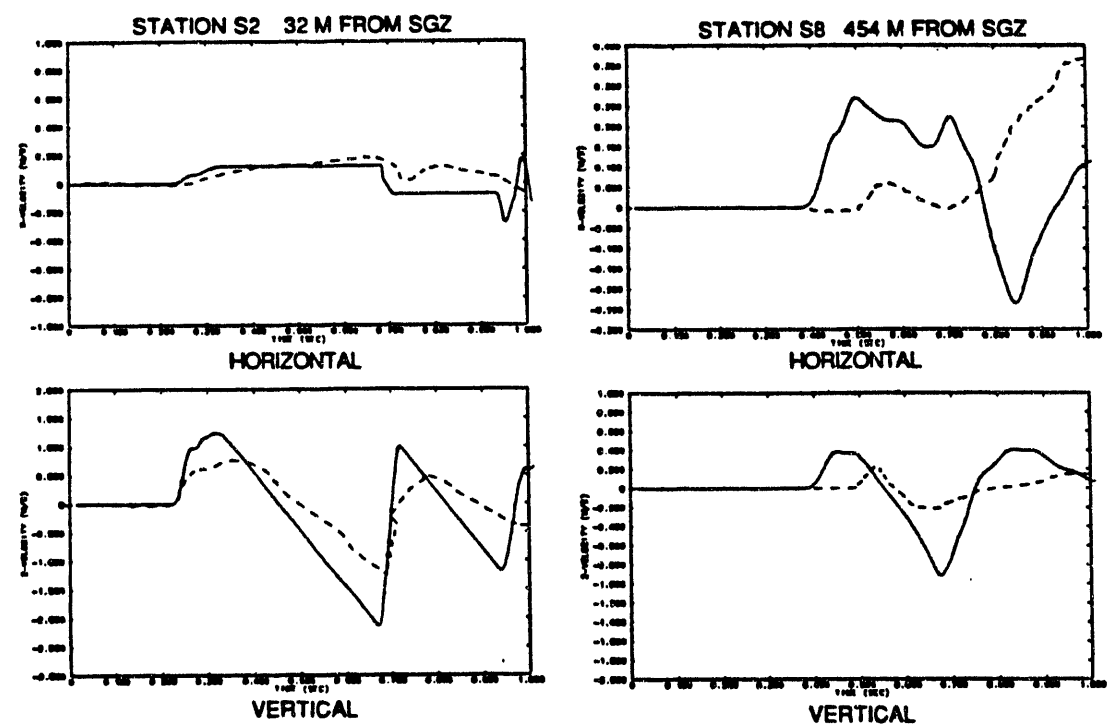

Figure 9. Comparison of calculated (solid) vs measured (dashed) horizontal and vertical free surface velocity waveforms at Stations S2 and S8. MERLIN Case A.

Figure 10 shows spall contours for the higher strength case at the same times as Figure 5 (Baseline Case). Spall is more definite and of greater extent for Case A. The maximum kinetic energy within the spall region is 8.7 GJ (~2.1 tonnes). This is about 2.4 times the spall energy of the Baseline Case and represents about .02 percent of the total explosive energy of the MERLIN device. The total kinetic energy in the elastic field (remember the caution) is about 62 GJ (~14.8 tonnes - 0.15 percent of the MERLIN yield), so in this case the energy potentially available for generation of seismic signals from spall closure is about one-seventh of that available for seismic waves radiating from the point source explosion.

Case A shows that surface motion, spall and "pseudospall" are very sensitive to relatively small changes in strength of the alluvium. Also, the results suggest that to attain better agreement with the data, strengths even lower than used in the Baseline Case should be used in the modelling.

Case B - Deeper WP (400 m) - same SDOB (Yield=24.7 kt). Here, the objective is to look at scale effects and determine the physical mechanisms (or computational inadequacies) responsible for any deviations from our standard scaling assumptions. The waveforms are time delayed from the Baseline Case by about 60 ms because of the increased ranges to the editing stations. The only stations at the same scaled range as the Baseline Case are those at the surface near SGZ.

Figure 11 shows the calculated and measured particle velocity waveforms to a depth of 92 m. Comparing to Figure 2, we observe that the waveforms are similar to those of the Baseline Case. At the surface, the onset of spall relative to the first arrival is delayed compared to the Baseline but once started it is slightly stronger and more definite. Figure 12 should be compared to Figure 4. Increasing both the depth and yield in this manner broadens the signal at the surface.

Figure 13 shows spall contours for the higher yield case at times shifted by 60 ms from those of Figure 5 (Baseline Case). The onset of spall is delayed compared to the Baseline (no spall before 540 ms) but once started it is more definite and occupies a larger volume. The first spall occurs subsurface. At 680 ms, the time equivalent to 620 ms in Figure 5, the spall zone is beginning to close but does not fully close until about 800 ms, long after the Baseline Case. The maximum kinetic energy within the spall region is 8.4 GJ (~2.0 tonnes). This is 2.3 times the spall energy of the Baseline Case, almost exactly the same as the yield ratio. The total kinetic energy in the elastic field is about 115 GJ (~27.5 tonnes). The ratio of energy in the elastic field to explosive yield is higher (0.11 percent) in this case

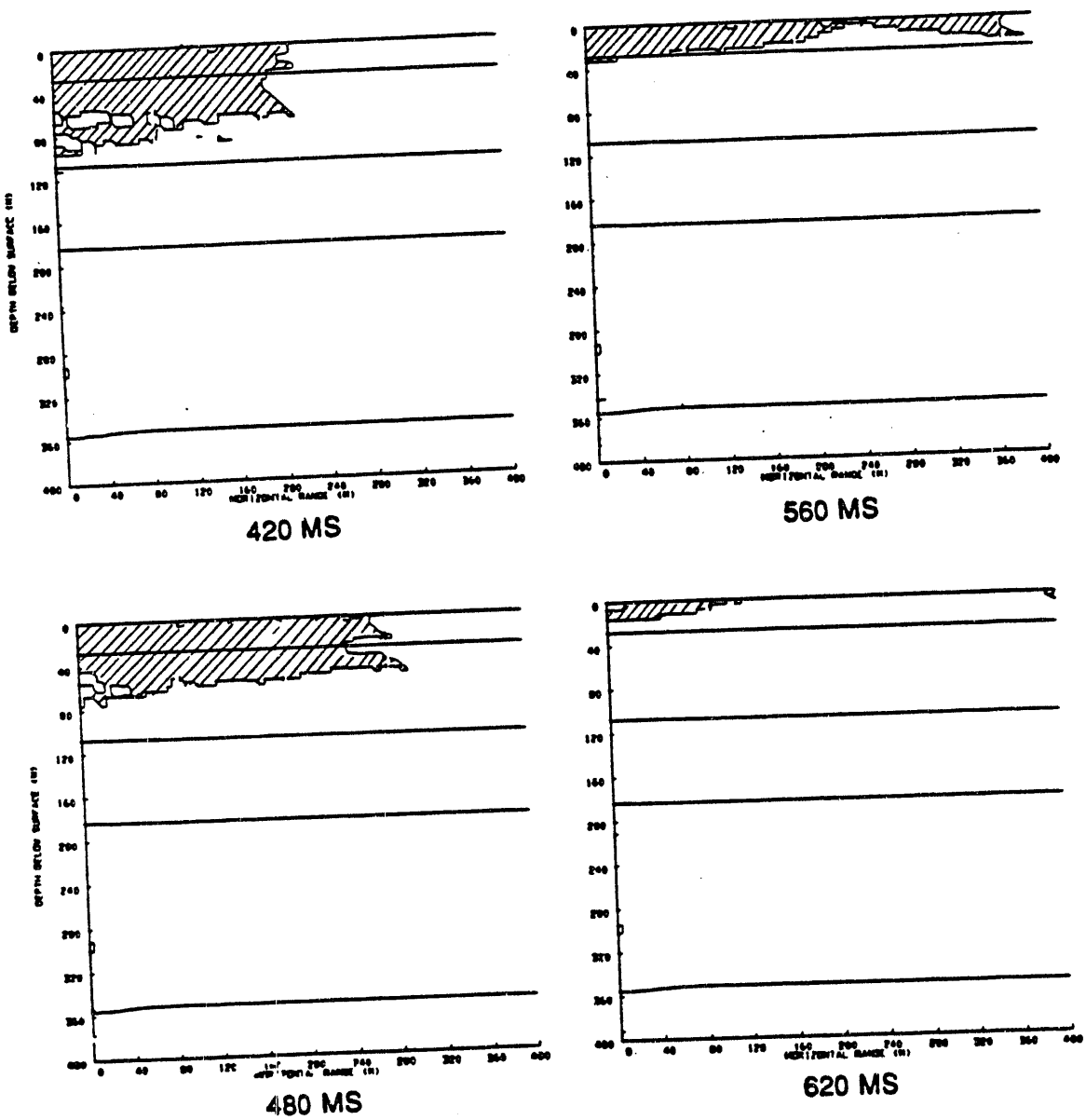

Figure 10. Evolution of spall from 420 to 620 ms. MERLIN Case A. Regions of zero stress (spall) are hatched.

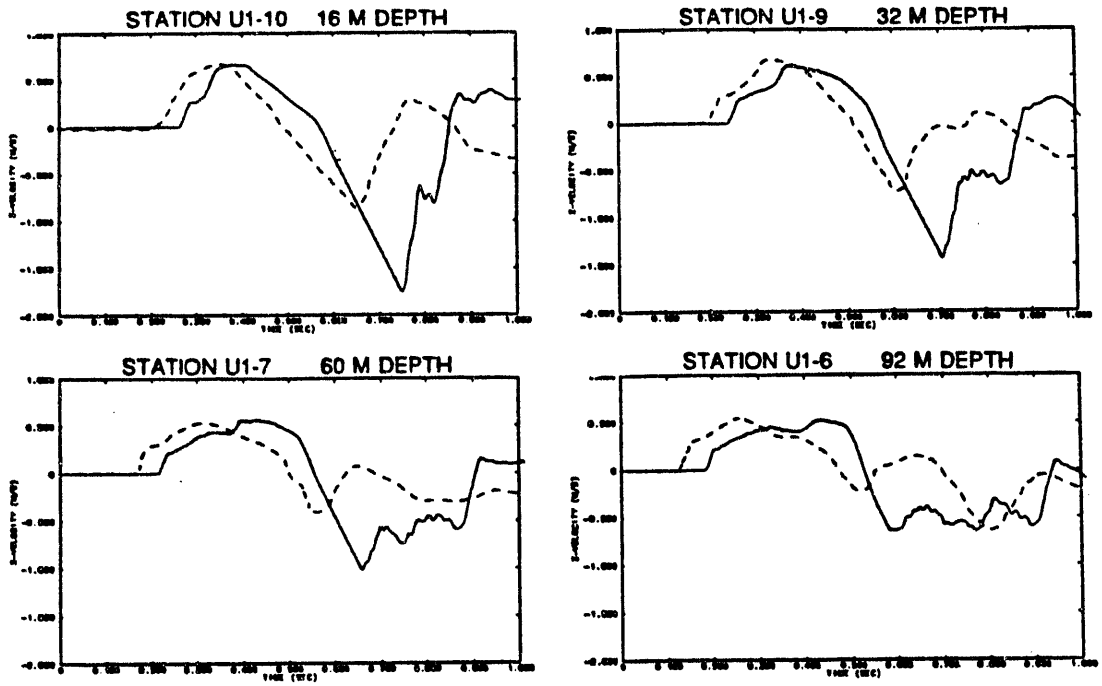

Figure 11. Comparison of calculated (solid) vs measured (dashed) particle velocity waveforms from 16 to 92 m depth. MERLIN Case B.

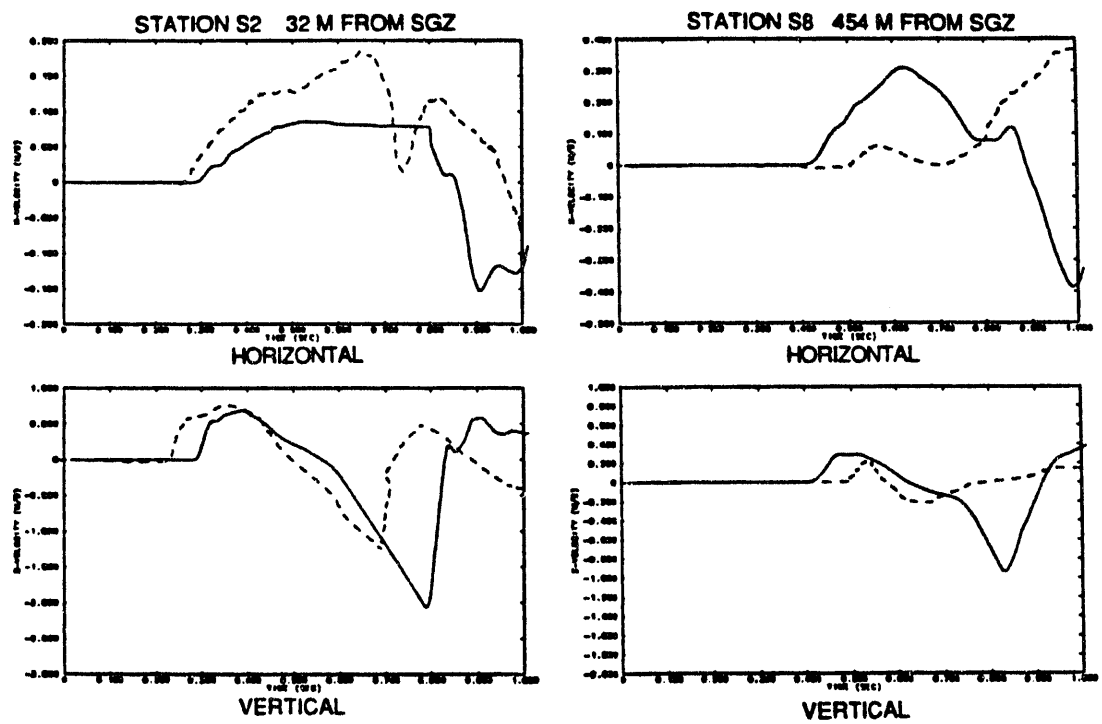

Figure 12. Comparison of calculated (solid) vs measured (dashed) horizontal and vertical free surface velocity waveforms at Stations S2 and S8. MERLIN Case B.

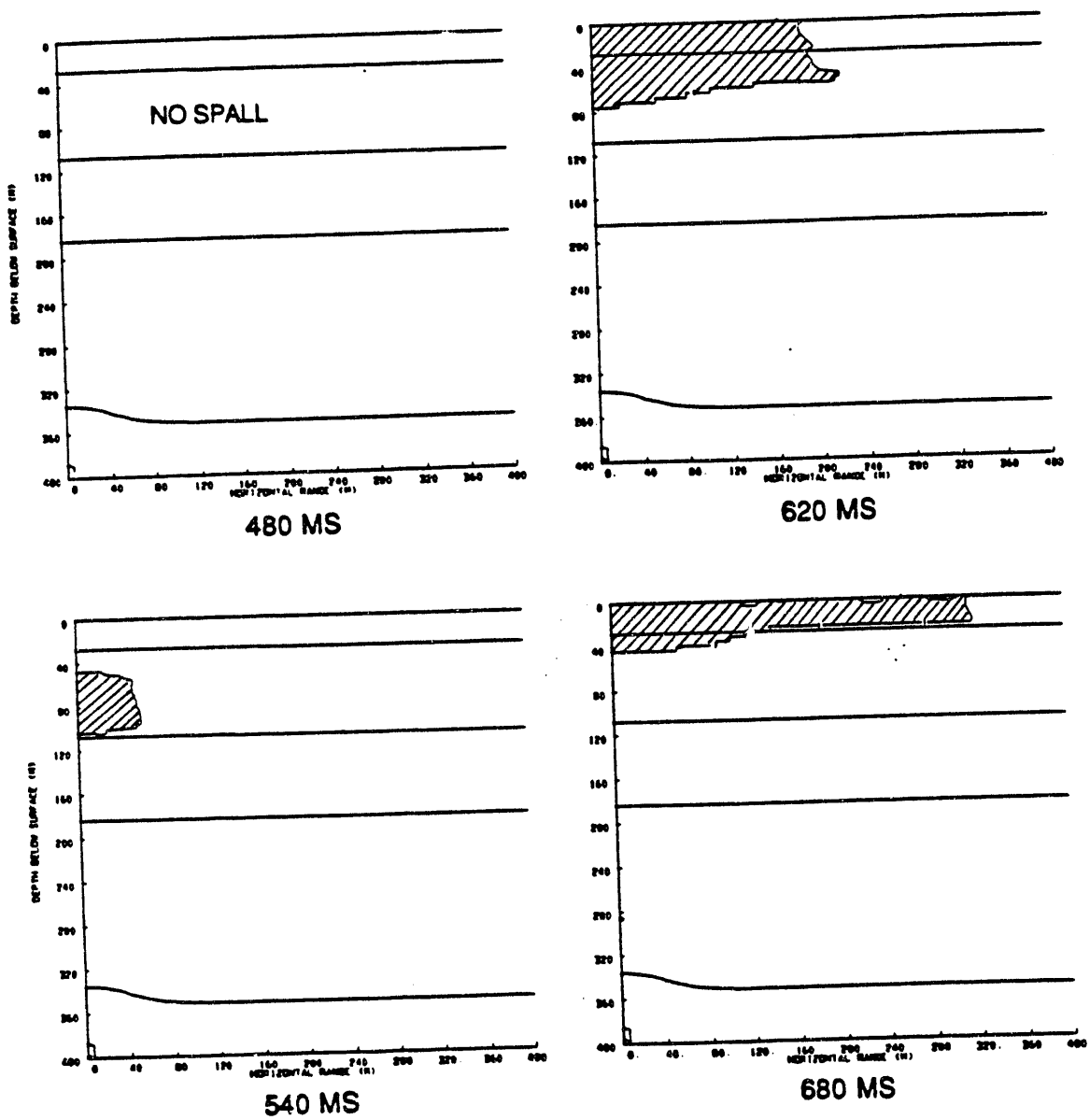

Figure 13. Evolution of spall from 480 to 680 ms. MERLIN Case B. Regions of zero stress (spall) are hatched.

than for the Baseline (.08 percent), a somewhat surprising result that may be physical (deeper in the section) or may be due to the less-than-perfect energy editing procedure discussed above. If it is a real effect, it may have implications for teleseismic observations.

Case C - Deeper WP (400 m) - MERLIN yield (SDOB=185.7). Here the objective is to look at the effect of overburial on surface motion and spall. Again, bear in mind that all waveforms are time delayed by about 60 ms because of the greater depth of burial.

Figure 14 shows the calculated and measured particle velocity waveforms to a depth of 92 m. Figure 15 shows the surface motions. The only points to be made here are that the wave shapes are changed very little from the Baseline Case; only the amplitudes and onset and duration of spall are different and the differences are as expected.

Figure 16 shows spall contours for Case C, at times shifted by 60 ms from those of Figure 5 (Baseline Case) but at the same times as Figure 13 (Case B). Spall is shallower but of greater lateral extent than for the Baseline Case. It is shallower near SGZ because of the greater SDOB; it has greater lateral extent probably because of the higher angle of incidence at any given surface point away from SGZ. The maximum kinetic energy within the spall region is 3.5 GJ (~0.8 tonnes), very nearly the same as for the same yield at a shallower depth. The total kinetic energy in the elastic field is about 57 GJ (~13.6 tonnes), about 60 percent greater than for the Baseline Case and consistent with the observation made above for Case B that there may be a depth effect on coupling into the elastic field.

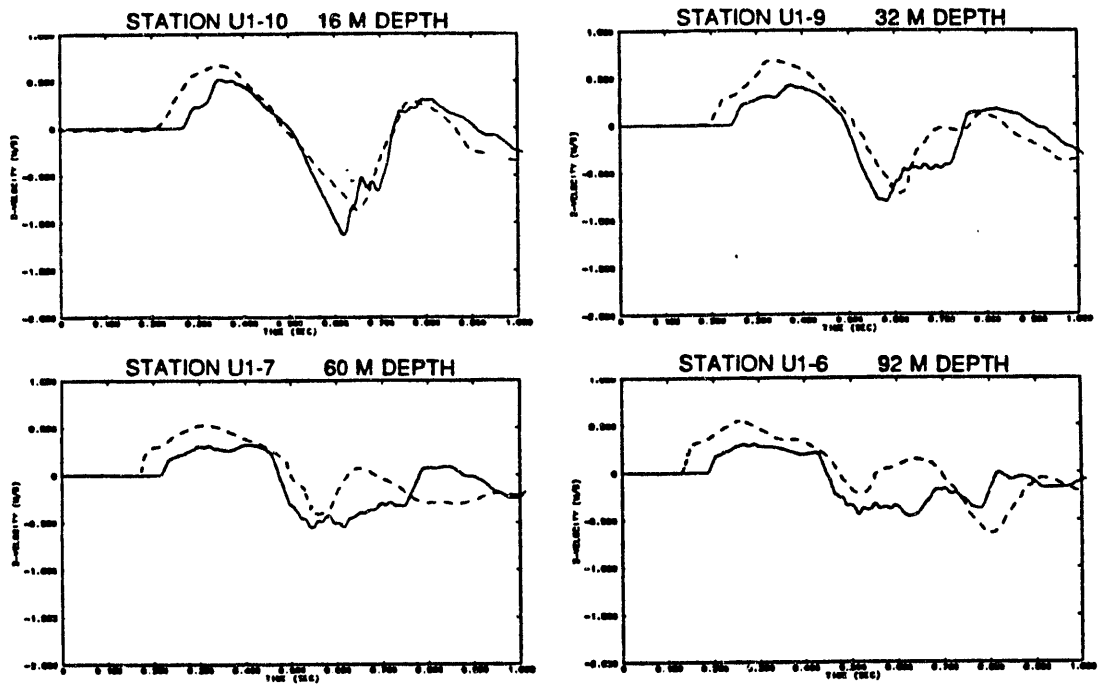

Figure 14. Comparison of calculated (solid) vs measured (dashed) particle velocity waveforms from 16 to 92 m depth. MERLIN Case C.

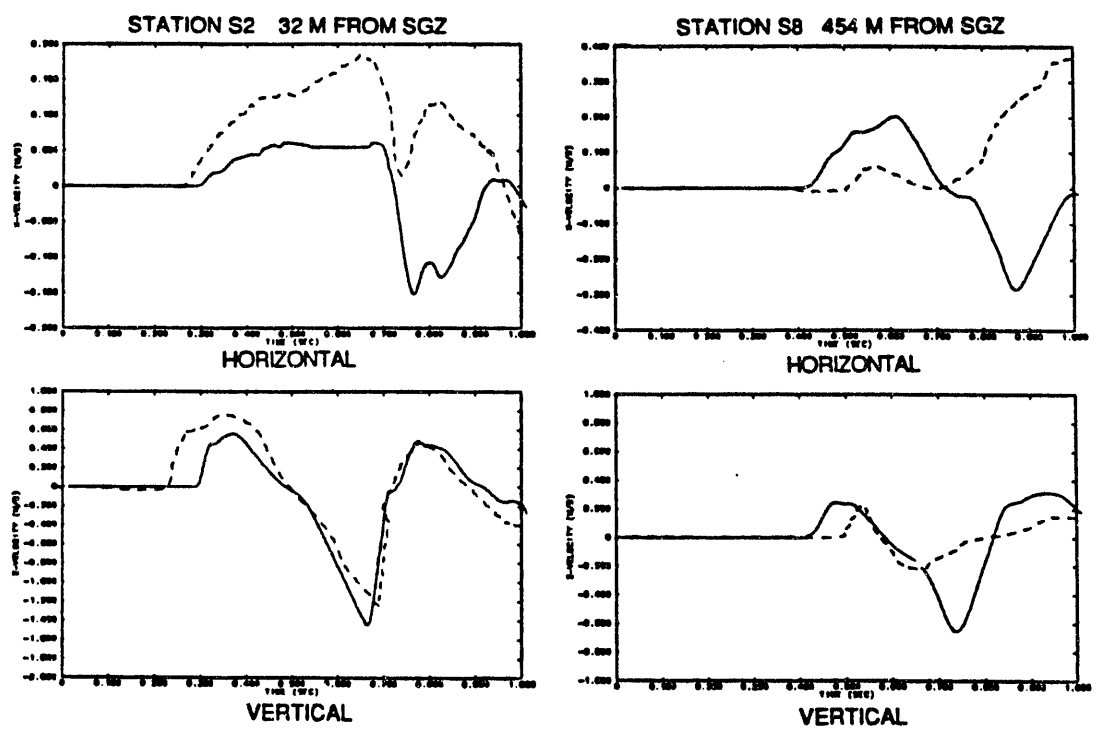

Figure 15. Comparison of calculated (solid) vs measured (dashed) horizontal and vertical free surface velocity waveforms at Stations S2 and S8. MERLIN Case C.

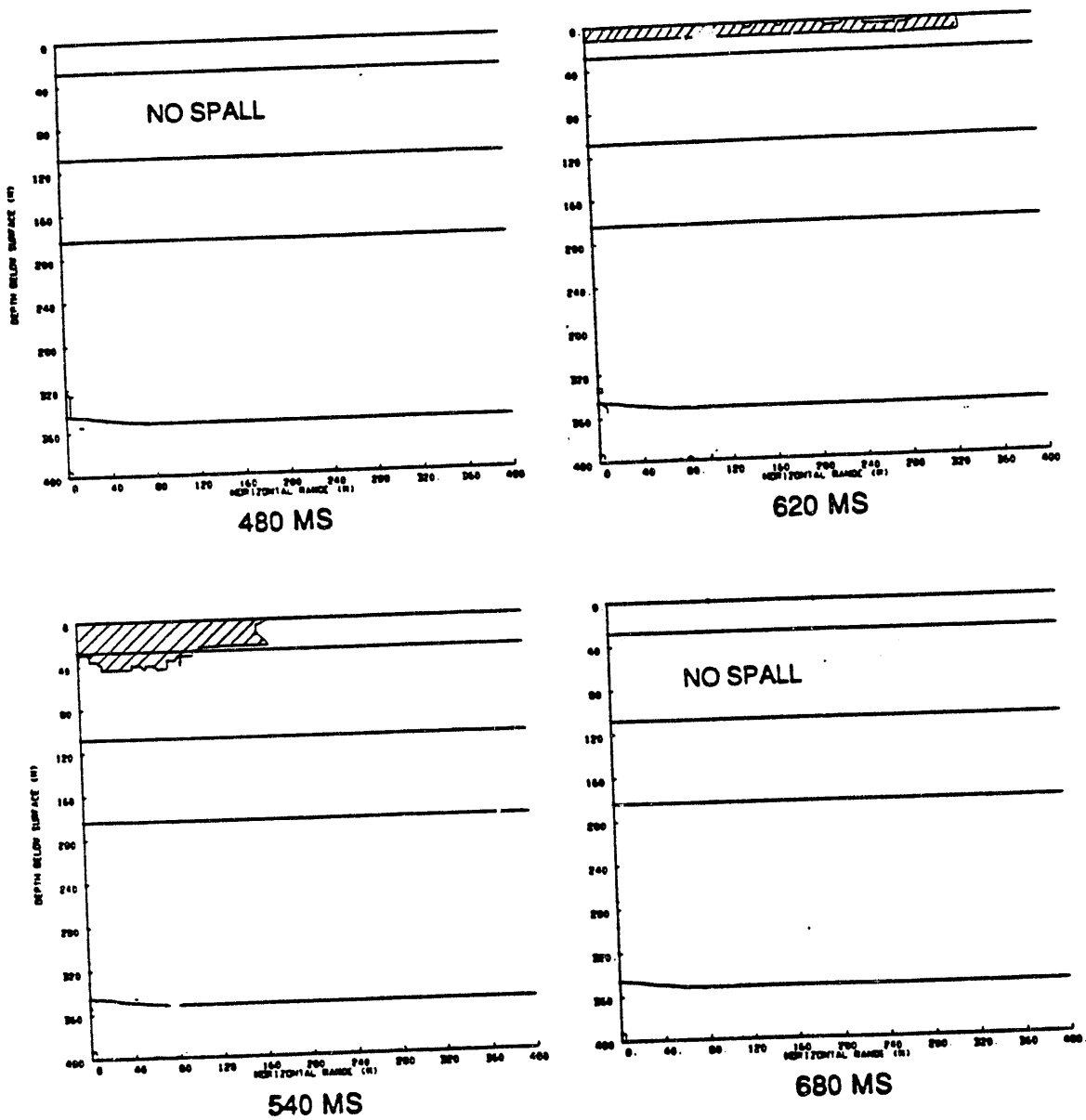

Figure 16. Evolution of spall from 480 to 680 ms. MERLIN Case C. Regions of zero stress (spall) are hatched.

HEARTS - An Intermediate Yield Event Conducted in Tuff Beneath the Water Table with Alluvium at the Surface.

Figure 17 shows the subsurface and surface motion station locations for HEARTS plus the stratigraphic section as it was broken out for the modelling. This nominal yield event was conducted beneath the water table in moderately dense tuff at a depth of 640 m. The stratigraphic sequence is comprised of an interlayering of tuffs ranging from weak and friable to strongly welded, all overlain by a 298 m thick section of alluvium. Table I describes in more detail the stratigraphy as it was used in the modelling along with values of bulk density, gas filled porosity and qualitative descriptions of the compressibilities and shear strengths. The motion data was collected by Los Alamos. Figure 18 shows the measured vertical particle velocity waveforms positioned by range from the WP. Lines 1 and 2 follow the first arrival and the peak of a "later phase". The reader will note that line 2 appears to be offset to the right of the points on the waveforms. The line is formed by projecting the point on the waveform vertically down to intersect the range at which the measurement is taken. The propagation velocity of the later phase is about 1000 m/s, close to the mean bulk sound speed of the alluvium. The significance of this "later phase" is discussed below. The tuff/alluvium interface is at 342 m range, 12 m below Station 4. Note the rapid change in character of the waveform that occurs between Stations 4 and 3. Figure 19 shows a similar plot (less Station 3) but with the waveforms from the Baseline Case calculation superposed on the measurements. There is good qualitative agreement between calculations and measurements. Both show the severe attenuation of the wave as it propagates through the deeper alluvium. Equally significant, the "later phase" is present in the calculation. The precise amplitude and period of the waveform at Station 4 is very sensitive to its distance above the interface, and the interface is known to slope between 10 and 15 degrees at this site. The fact that the calculated risetime is too short at that station is not a concern; a better match could be achieved simply by changing slightly the location of the interface (or the edit point). The noted attenuation is due to void crush and the fact that we achieve the requisite broadening in the calculation at the upper stations is a good indication that the crush response model we use for alluvium is basically sound. The main discrepancy between the calculation and measurements is in the rarefaction (reverse slope) part of the wave. The calculated broadening of the wave is not quite sufficient to delay spall enough to match the data. However, we believe we are capturing enough of the important physical mechanisms to allow us to proceed in analyzing surface motion and spall for HEARTS.

Events conducted beneath the water table in Yucca Flat generally have a "delayed" onset of spall near SGZ. Figures 20 and 21 compare the peak free surface accelerations and particle velocities at SGZ for HEARTS, TORTUGAS, CAPROCK and BASEBALL. All were

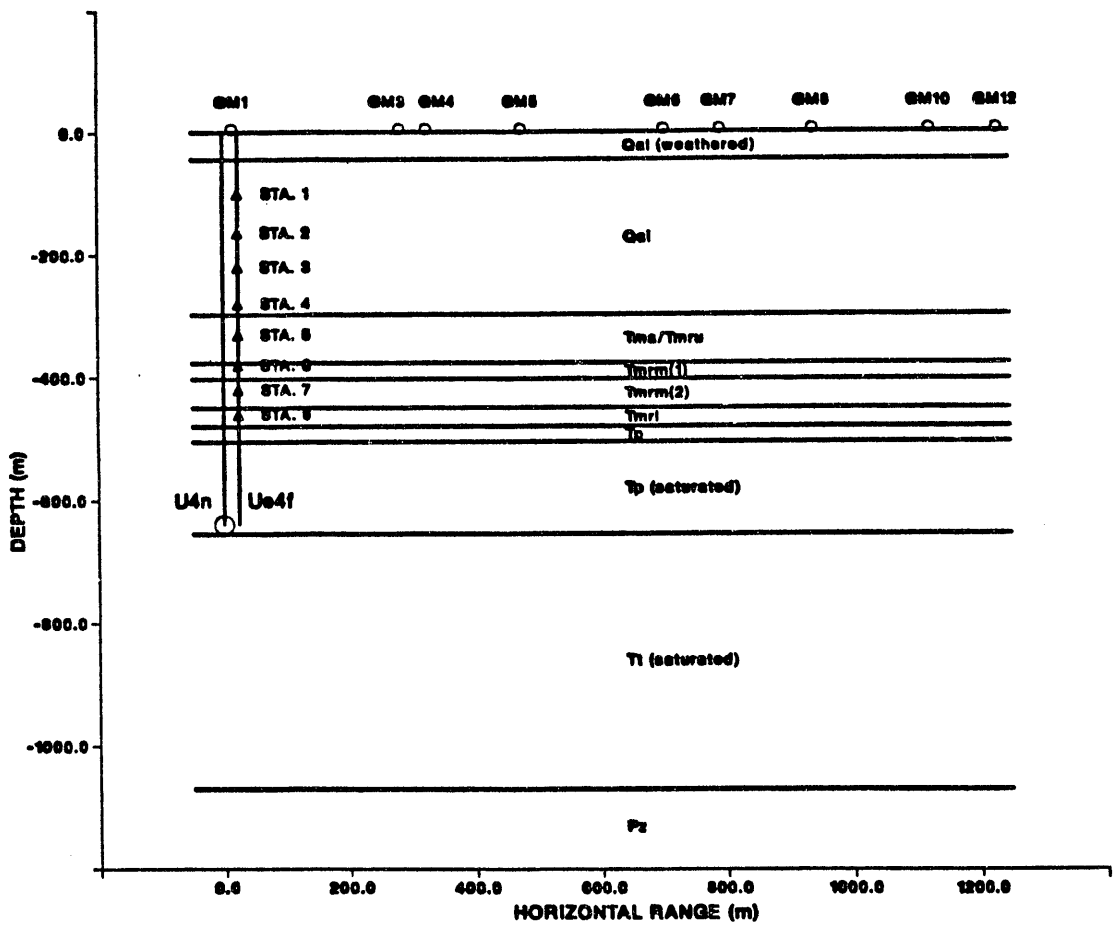

Figure 17. HEARTS ground motion station locations and stratigraphy as it was modelled in the Baseline Case. Triangles represent vertical accelerometer stations in satellite hole Ue4f. Circles represent three component surface accelerometer stations.

Table I

Modelled Stratigraphy at U4n - HEARTS

Unit	Depths(m)	Description (rho=bulk density in Mg/m^3, GFP=gas porosity in percent)
Qal	0-298	Tuffaceous alluvium - poorly indurated; rho=1.78; GFP=16; highly compressible. Upper 45 m modelled as low velocity weathered layer extremely weak in shear - rest of alluvium only slightly stronger.
Tma/ Tmru	298-377	Ammonia Tanks Member of Timber Mountain Tuff plus upper portion of Rainier Mesa Member of Timber Mountain Tuff - ash flow tuffs - non-welded; rho=1.95; GFP=5.7; moderately compressible; moderate shear strength.
Tmrm (1&2)	377-450	Middle unit of the Rainier Mesa Member - ash flow tuff - moderately (upper part) to densely (lower part) welded; rho=2.07; GFP=11 (upper); rho=2.22; GFP=4 (lower); very stiff in compression; high shear strength.
Tmrl	450-480	Lower part of Rainier Mesa Member - ash flow tuff - partially to moderately welded; rho=1.86; GFP=2; moderately compressible; weak in shear.
Tp	480-655	Paintbrush Tuff - reworked tuff - slight to moderate induration - zeolitized - water table at 505 m; rho=1.85; GFP=2 above water table; rho=1.88; GFP=0.5 below water table; relatively stiff due to low GFP; moderateshear strength.
Tt	655-1070	Tunnel Beds Tuff - reworked tuff - slightly indurated - zeolitized; rho=1.96; GFP=0; stiff in compression due to saturation; moderate shear strength (stronger than Tp).
Pz	1070-Base	Paleozoic rocks; rho=2.78, GFP=0, very stiff in compression, very high shear strength.

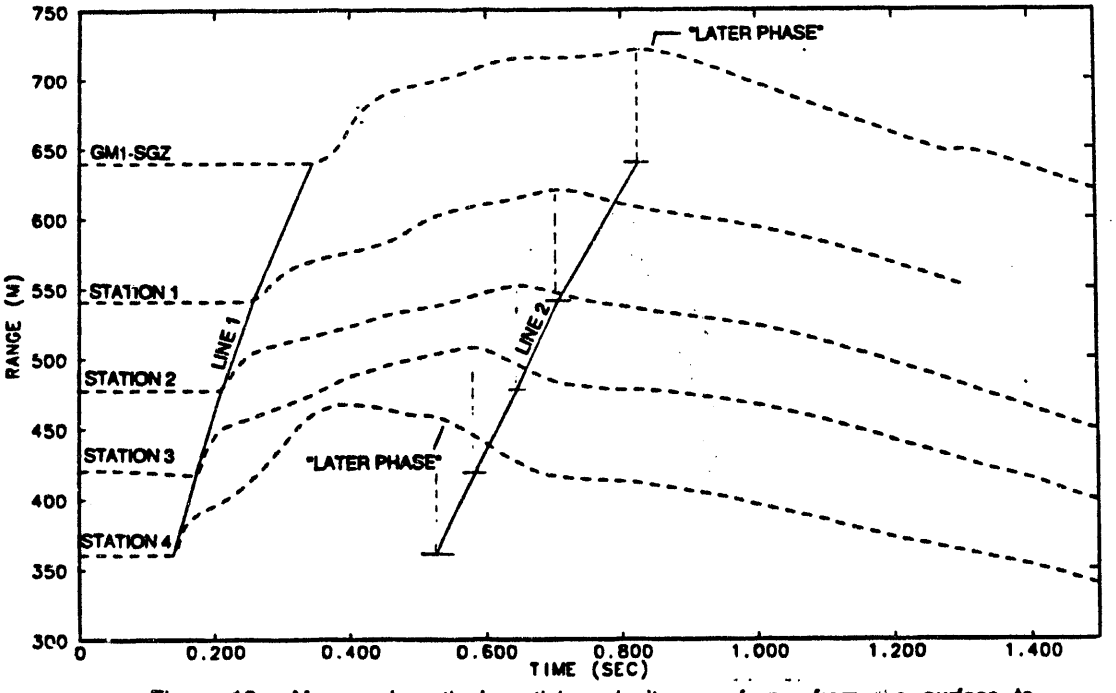

Figure 18. Measured vertical particle velocity waveforms from the surface to 280 m depth, positioned by range from the WP. HEARTS event. Line 1 tracks the first arrivals; line 2 tracks the peak of the upward propagating "later phase".

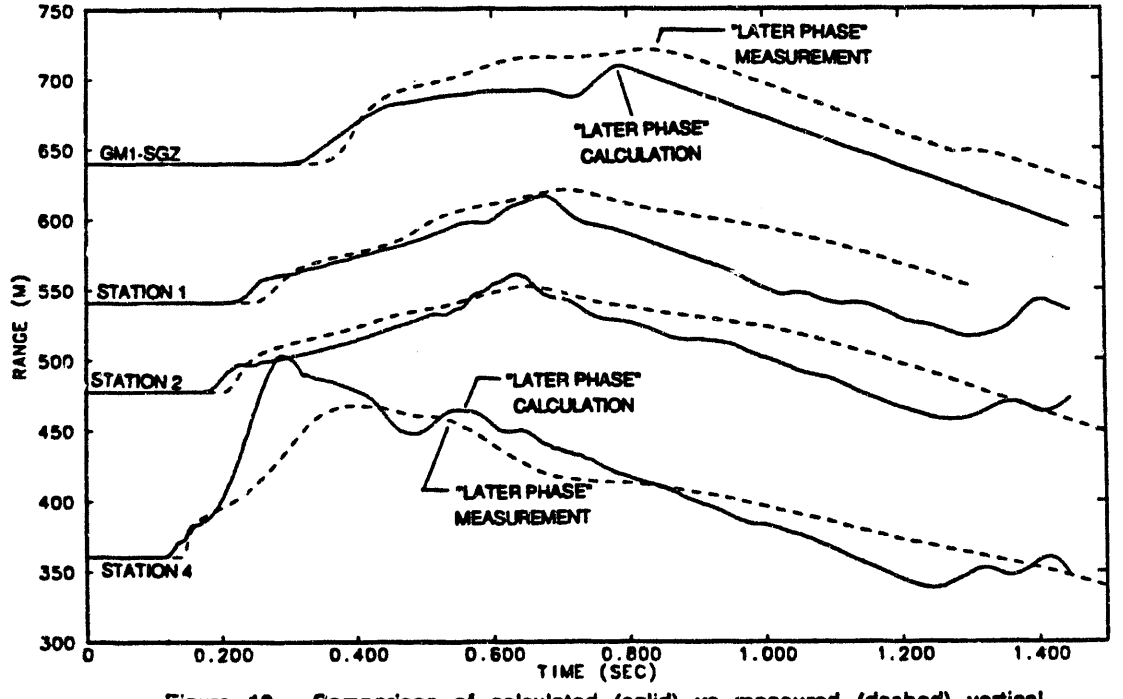

Figure 19. Comparison of calculated (solid) vs measured (dashed) vertical particle velocity waveforms from surface to 280 m depth, positioned by range from the WP. HEARTS Baseline Case.

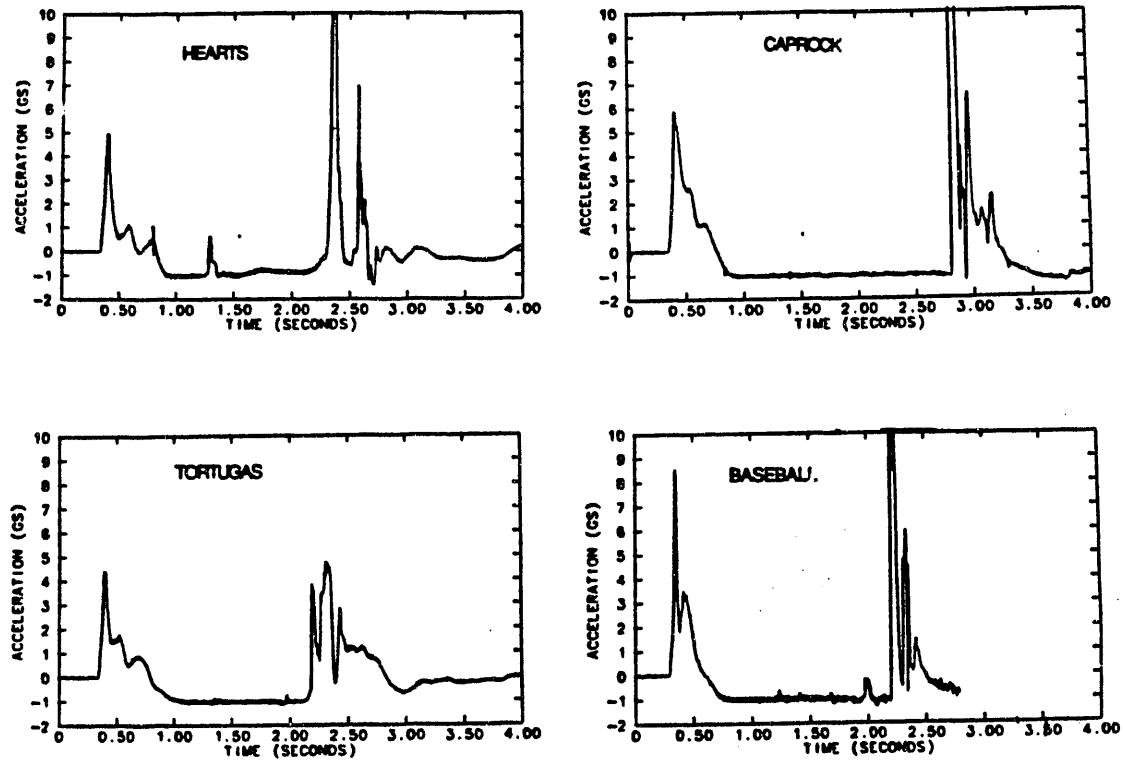

Figure 20. Comparison of SGZ vertical free surface accelerations for HEARTS, TORTUGAS, CAPROCK and BASEBALL.

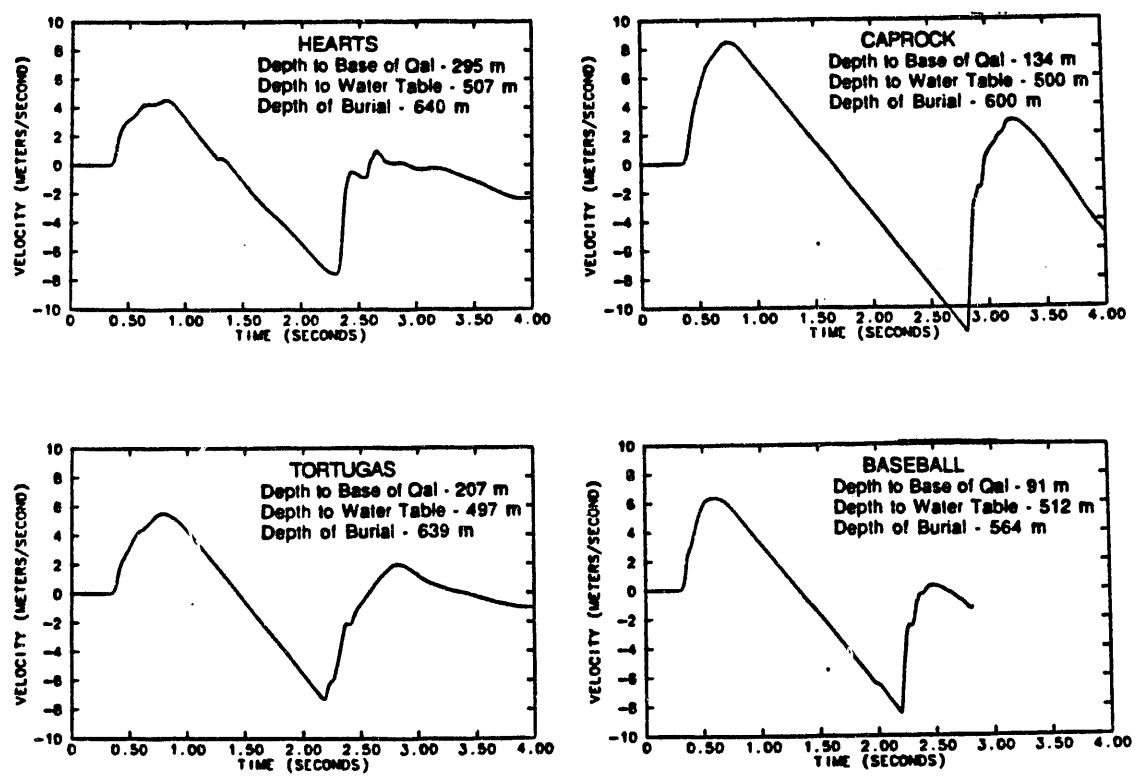

Figure 21. Comparison of SGZ vertical free surface velocities for HEARTS, TORTUGAS, CAPROCK and BASEBALL.

conducted beneath the water table, all had "similar" scaled-depths-of-burial and all were located within the same geologic structural block. What is different about them is the thickness of alluvium present at their respective sites and to a lesser extent, their relative depths beneath the water table. Some specifics are noted in Figure 21. Three of the waveforms (HEARTS, TORTUGAS and CAPROCK) show three distinct arrivals prior to spall. BASEBALL shows just two. Referring to Figure 20, the first and highest amplitude arrival is the elastic precursor. The second arrival is the elastic remnant of the inelastic (or plastic) wave, i.e., it is what is left over after the plastic wave decays to a point where the material is no longer deforming inelastically. In this paper, we shall refer to it as the "plastic remnant". For HEARTS, the third arrival corresponds to the arrival of the "later phase" identified as line 2 in Figure 18. For this selection of events, the time separation between arrivals increases with increased thickness of alluvial cover. For BASEBALL, it is possible that the second and third arrivals are coincident as suggested by the slightly more rounded peak of the velocity waveform. If these pulses are spread out as they are at HEARTS, the incident wavelength at the free surface is greater which can lead to deeper spall. If they are close together as they are at CAPROCK, they reinforce one another leading to high free surface velocity. Note that unlike MERLIN, which was conducted within the alluvium, spall acceleration is negative 1 g in all four cases.

In the HEARTS calculation, the "later phase" (third arrival) is generated by an elastic rebound of material from the side and beneath the cavity and focused inward and upward along the vertical axis of symmetry. Henceforth we will refer to this "later phase" as the rebound pulse. Figure 22 is a velocity vector plot taken at 600 ms. Each vector length is proportional to the particle velocity at that point. The arrows provide the sense of direction of flow. At 600 ms, the rebound pulse is arriving at Station 3 (Figure 18). At depth, the amplitude of this pulse is minute compared to the amplitude of the initial shock wave, but because it propagates as an elastic wave it suffers little attenuation and has significant amplitude relative to the other phases upon arriving at the surface. The sweeping motion is preferentially upward because of the lower overburden pressure and reduced impedance (sound speed, density) in that direction. All the factors that contribute to the rebound are not fully understood. In a companion study of DNA tunnel events (Brunish and App, 1991), we have indications that variations in the elastic moduli (longitudinal and shear velocities) with depth may be important.

Figure 23 shows the free surface particle velocities measured for HEARTS, positioned within the picture by range from SGZ. Figure 24 shows a subset of these free surface waveforms superposed with the calculated waveforms. There is a change in the character of the surface motion with increasing distance from SGZ. At SGZ the three distinct phases discussed above appear both in the calculation and measurements. With increasing distance from SGZ the surface waveform becomes more "N" shaped, a signature typically observed

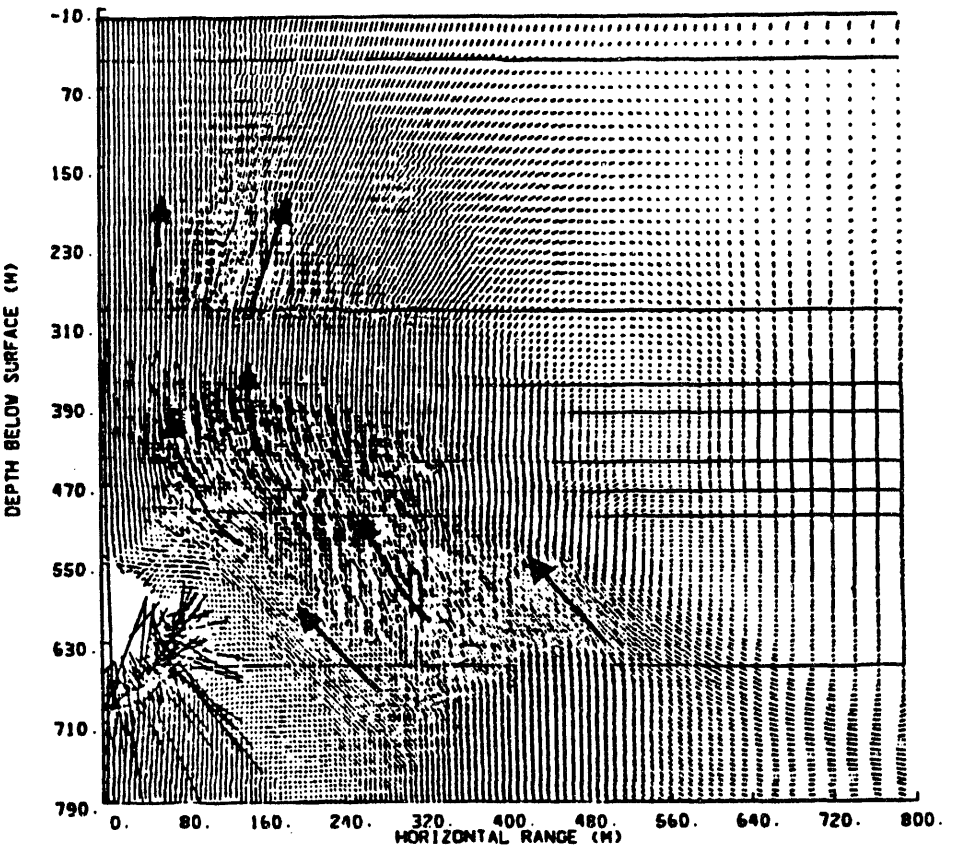

Figure 22. Velocity vector field at 600 ms. HEARTS Baseline Case. Vector lengths are proportional to the particle velocities. Heavy arrows show general direction of flow.

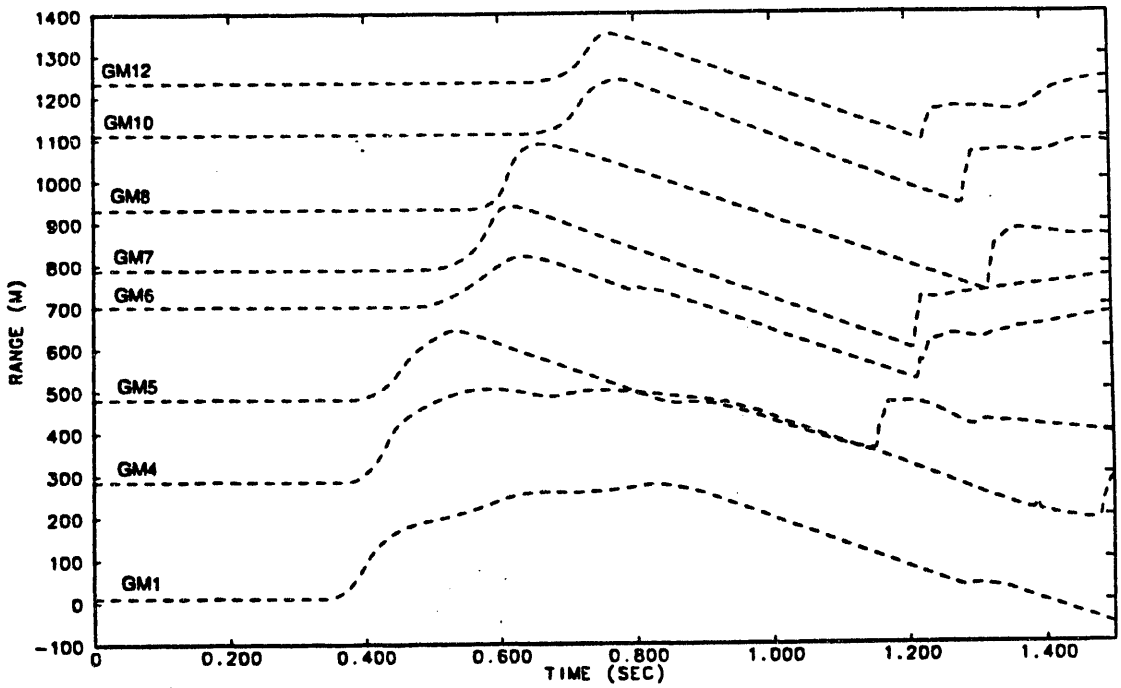

Figure 23. Measured vertical free surface particle velocity waveforms from SGZ to 1230 m range, positioned by range from SGZ. HEARTS event.

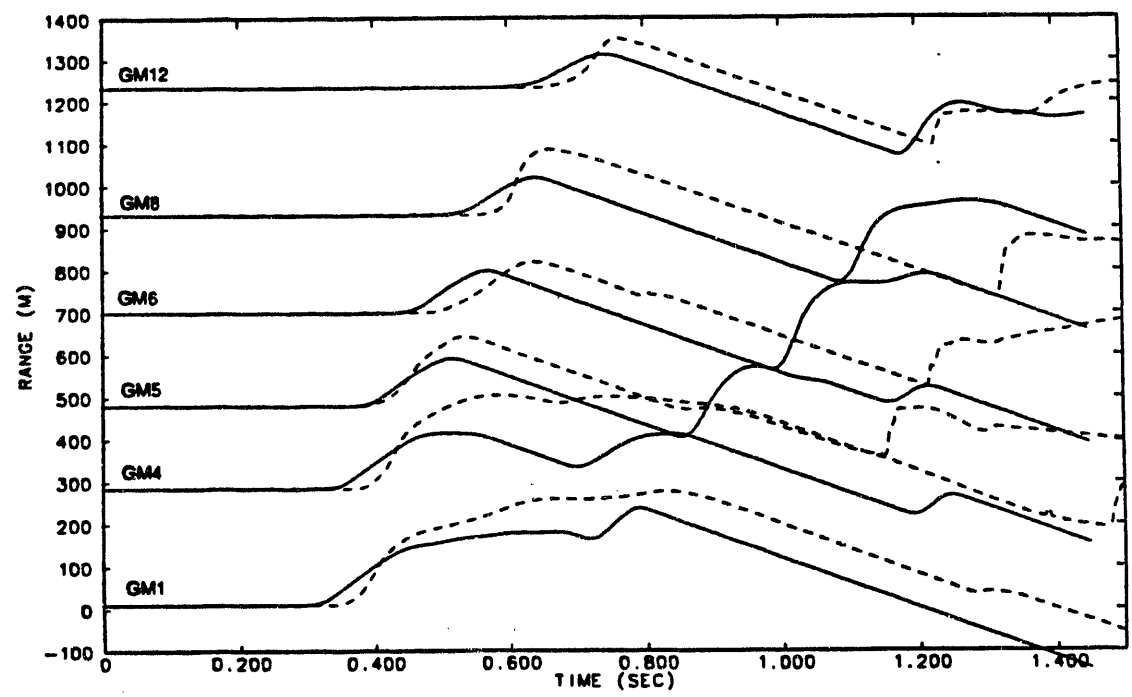

Figure 24. Comparison of calculated (solid) vs measured (dashed) vertical free surface particle velocity waveforms from SGZ to 1230 m range, positioned by range from SGZ. HEARTS Baseline Case.

near SGZ at sites without overlying alluvium, such as Pahute Mesa. An "N" shape results when spall immediately follows the elastic precursor. At GM4 the calculated waveform exhibits a double peak that agrees in timing but not amplitude with the measurement. Examination of the plastic remnant at a subsurface edit point 163 m below GM4 shows that it is poorly developed, thus it is relatively ineffective in delaying spall at the surface. Spall begins early at GM4 (relative to GM1) and then is interrupted by the arrival of the rebound pulse, resulting in the double peaked waveform. A similar examination at 163 m depth below GM7 (not included in Figure 28 but located between GM6 and GM8) revealed that there is no discernible plastic remnant at that location; therefore spall begins immediately after surface reflection of the elastic precursor and the surface waveform is "N" shaped. The calculated first spall closures occur too early at Stations GM5 through GM8 but they do show the same trend of successively later spall closure with increasing distance from SGZ that is observed in the data. At these stations it appears that the calculation is misrepresenting the strength and timing of the rebound pulse. At the farthest station (GM12) the duration of spall and time of closure are very near the measured values.

Figure 25 is a two-dimensional representation showing the evolution of spall for HEARTS. At 600 ms the surface is in spall between 300 and 700 m surface range from SGZ. Spall first started between 400 and 550 m range at 550 ms (not shown) and grew inward and outward from there. This pattern of evolution is consistent with the measurements; spall first occurred at GM5, 476 m from SGZ. In the calculation, the spall briefly reaches a maximum depth of about 220 m directly beneath SGZ at 710 ms. This too is in good agreement with the measurement which indicates a very brief (~90 ms) period of spall at the 220 m depth (Station 3), starting at 600 ms. Because of the selection of snapshot times, Figure 25 does not show the deepest spallation. However there is even more to it than this. Beneath SGZ, a very large rarefaction region (less than 1 MPa compressive stress) develops to the base of the alluvium (298 m) at about 700 ms and persists until 1.2 sec. In Figure 25 this is shown as a lightly stippled region. The alluvium very nearly spalls to a depth of 298 m, almost one-half DOB. It is obvious from the velocity field plot (Figure 22) that the rebound pulse contributes significantly to the depth of the rarefaction. Actual spall is inhibited by the same mechanism that inhibited spall on MERLIN; i.e., the weak alluvium continues to fail in shear following surface reflection. The maximum spall associated kinetic energy is at 1.1 sec. and amounts to about 0.086 percent of the energy of the explosion. The total energy radiated as elastic waves from the point source explosion is 0.320 percent, so the energy potentially available from the spall zone as a second source for seismic waves is about one-fourth that potentially available from the explosion itself.

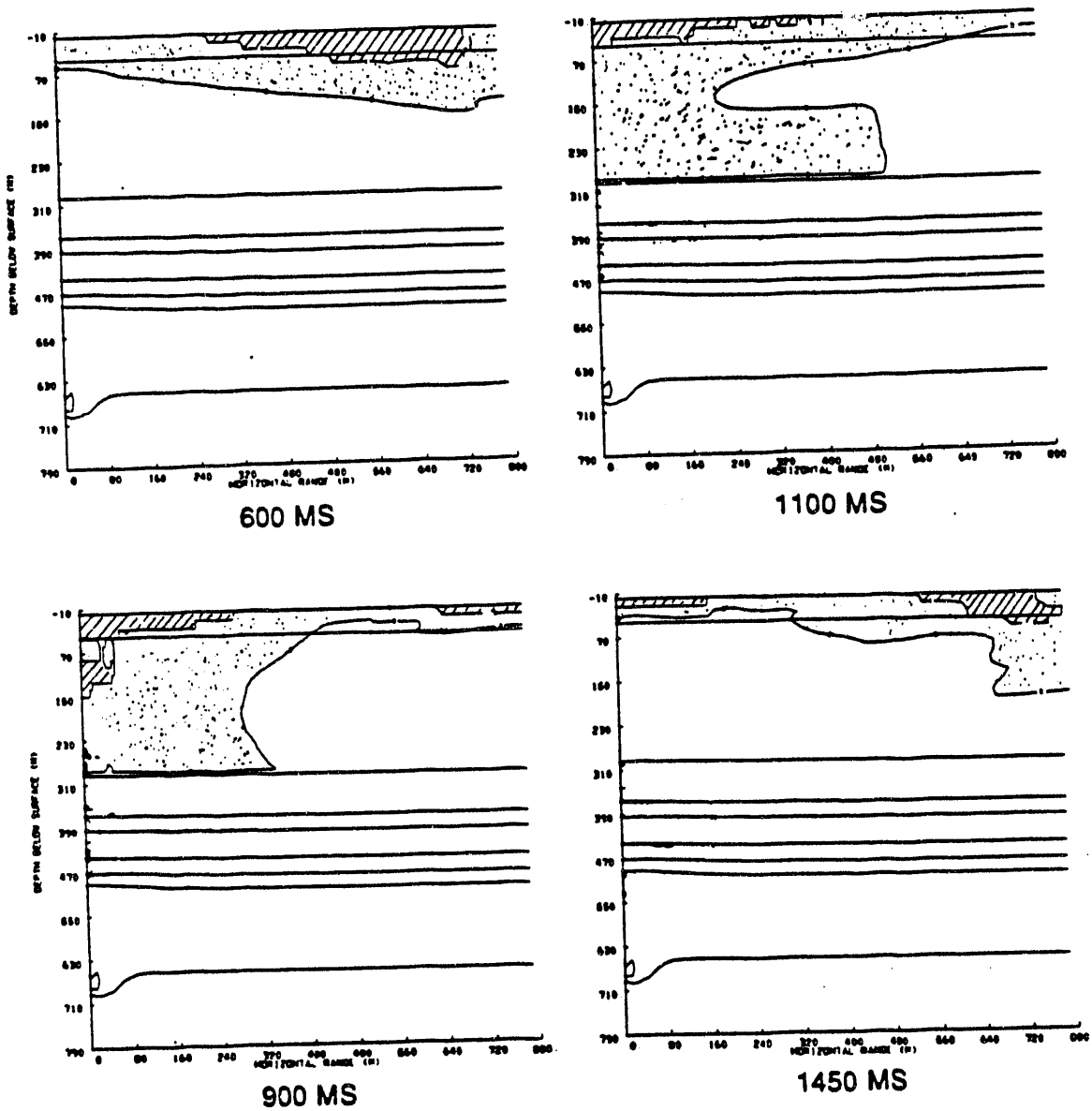

Figure 25. Evolution of spall from 600 to 1450 ms. HEARTS Baseline Case. Regions of zero stress (spall) are hatched; regions of very low compressive stress (less than 1 MPa) are stippled.

HEARTS Parameter Studies.

Case A - Deeper Water Table (Unsaturated WP). In the Baseline Case we modeled the WP rock with 0.5% gas filled porosity (GFP). We did this simply to achieve agreement with the measured amplitudes deep in the section. This was addressed in the earlier HEARTS report (App, Brunish and Edwards, 1989). Here we increase the GFP to 2%, the apparent gas porosity of rocks just above the water table at the HEARTS site. All other parameters are unchanged, including the shear strength of the rock which normally would increase with a reduction in water content and saturation.

Figure 26 shows the calculated vs measured waveforms in the alluvial section. Comparing this to Figure 19, we see that the rebound pulse either is missing or not distinct enough to identify. However there still is a delayed spall at SGZ due to the plastic remnant. Along the surface (Figure 27) we observe the same transition from delayed spall to an "N shape" that was observed in the "baseline" calculation. Figure 28 shows the velocity field at 600 ms. There is not the same degree of rebound-associated upward motion that we observe in the Baseline Case (Figure 22), suggesting that the rarefaction generated at a water table has a strong influence on the timing and magnitude of the rebound.

Figure 29 shows the evolution of spall, to be compared with Figure 25. Again the region of very low, but still compressive, stress is stippled. The spall patterns are similar but the stippled regions are much different. The maximum kinetic energy associated with spall is 0.046 percent, 46 percent less than the Baseline Case, so despite the similar appearance of the spall patterns, spall was much less energetic in Case A. The energy radiated as elastic energy from the explosion is 39 percent less than the Baseline Case. The high sensitivity of both spall kinetic energy and elastic kinetic energy to a change in rock compressibility is consistent with the MERLIN Case A result.

Case B - Less Alluvium. Earlier, in describing the SGZ motions for HEARTS, TORTUGAS, CAPROCK and BASEBALL (Figures 20 and 21), we noted the apparent influence of the thickness of the alluvium on the time of arrival of two distinct pulses following the elastic precursor. This calculation attempts to simulate the effect by reducing the thickness of the alluvium above the HEARTS WP to 125 m (from 298 m). The Ammonia Tanks (Tma) and the Rainier Mesa (Tmr) Tuff units also are moved up and the Paintbrush Tuff (Tp) is thickened by 173 m to make up for the thinner alluvium. Mechanical and physical properties of the stratigraphic units are unchanged.

Figure 30 shows the subsurface calculated vs measured waveforms. The measurements are included only as points of reference; the calculated waveforms are at the same ranges

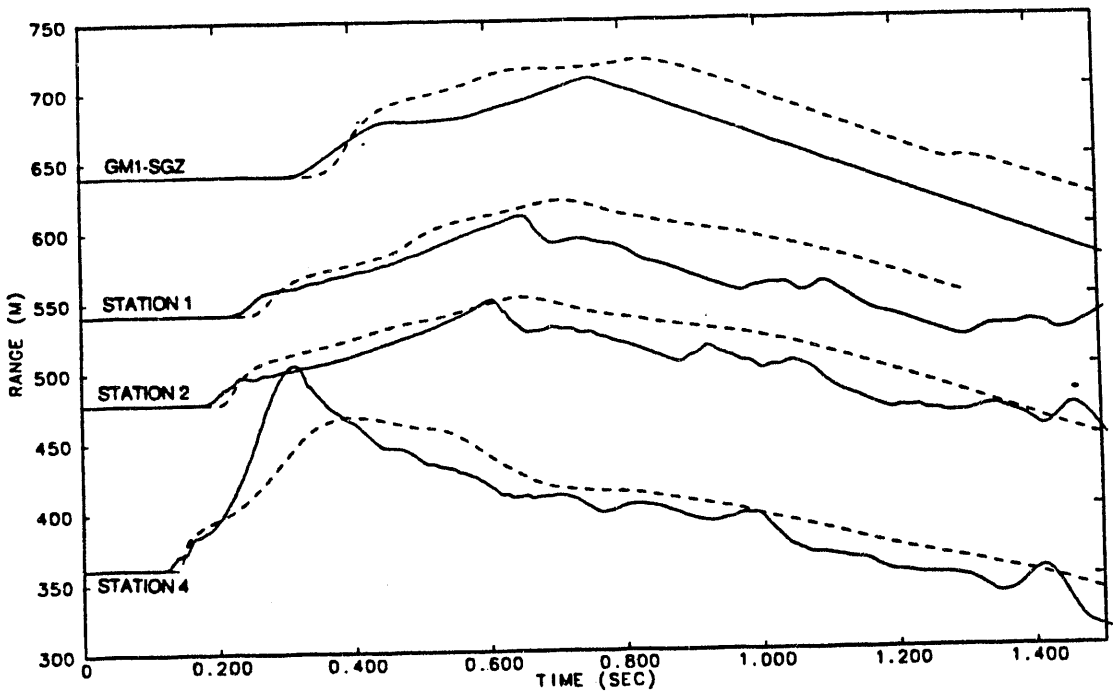

Figure 26. Comparison of calculated (solid) vs measured (dashed) vertical particle velocity waveforms from surface to 280 m depth, positioned by range from the WP. HEARTS Case A.

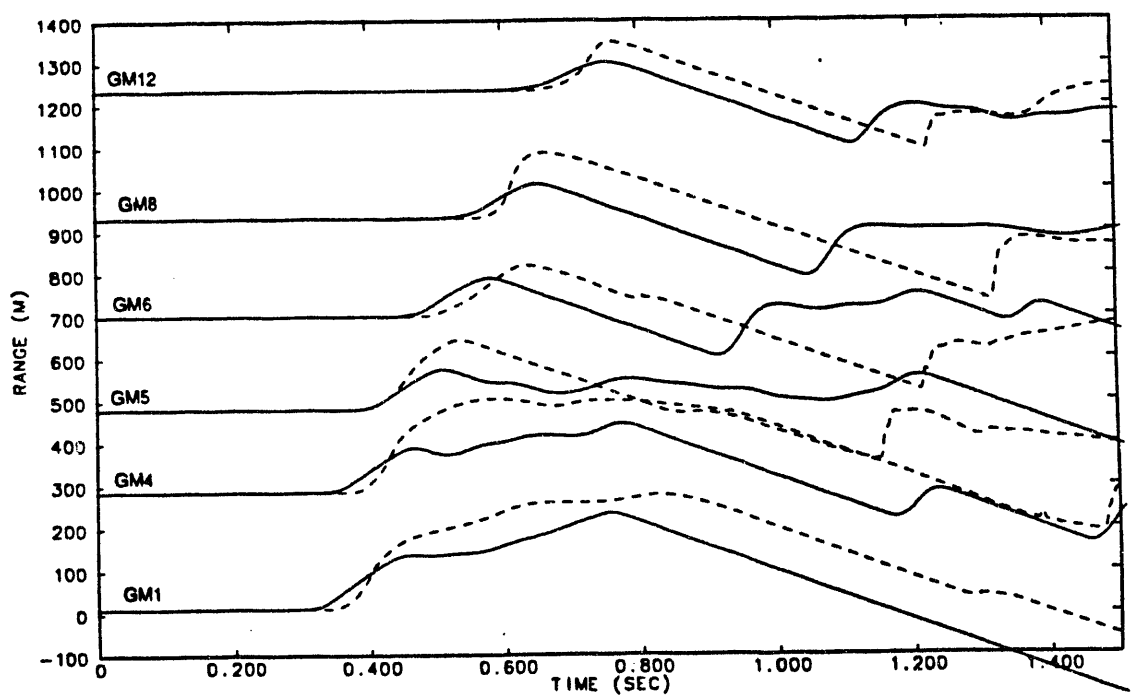

Figure 27. Comparison of calculated (solid) vs measured (dashed) vertical free surface particle velocity waveforms from SGZ to 1230 m range, positioned by range from SGZ. HEARTS Case A.

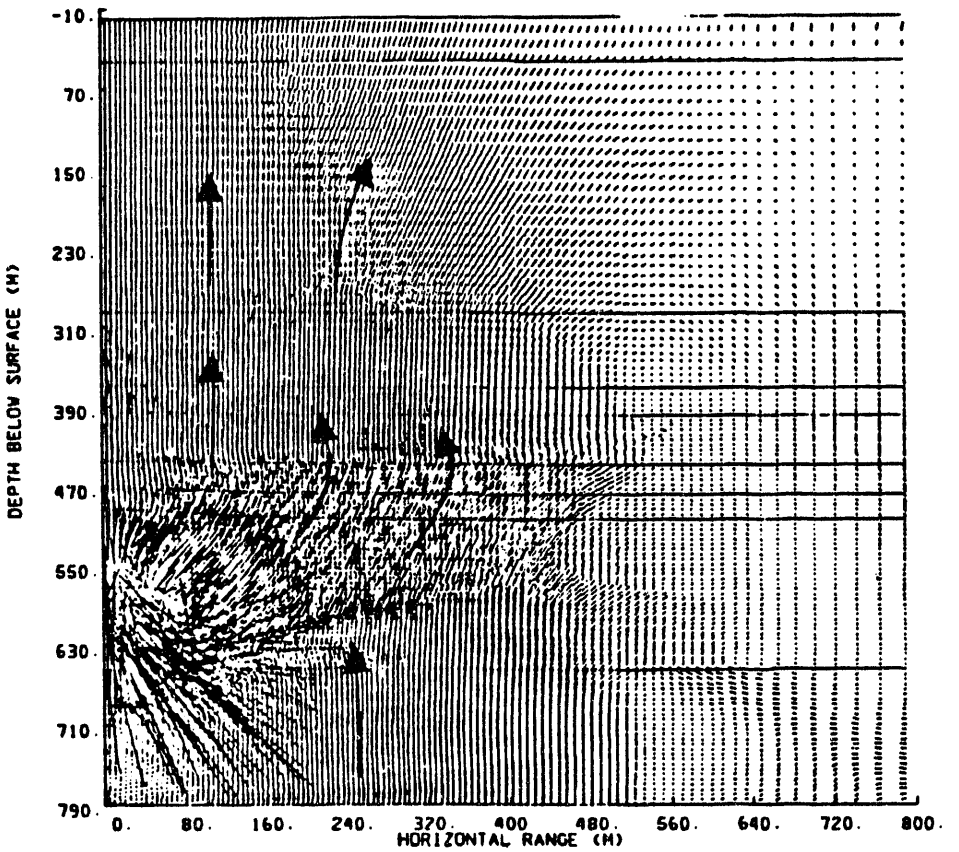

Figure 28. Velocity vector field at 600 ms. HEARTS Case A. Vector lengths are proportional to the particle velocities. Heavy arrows show general direction of flow.

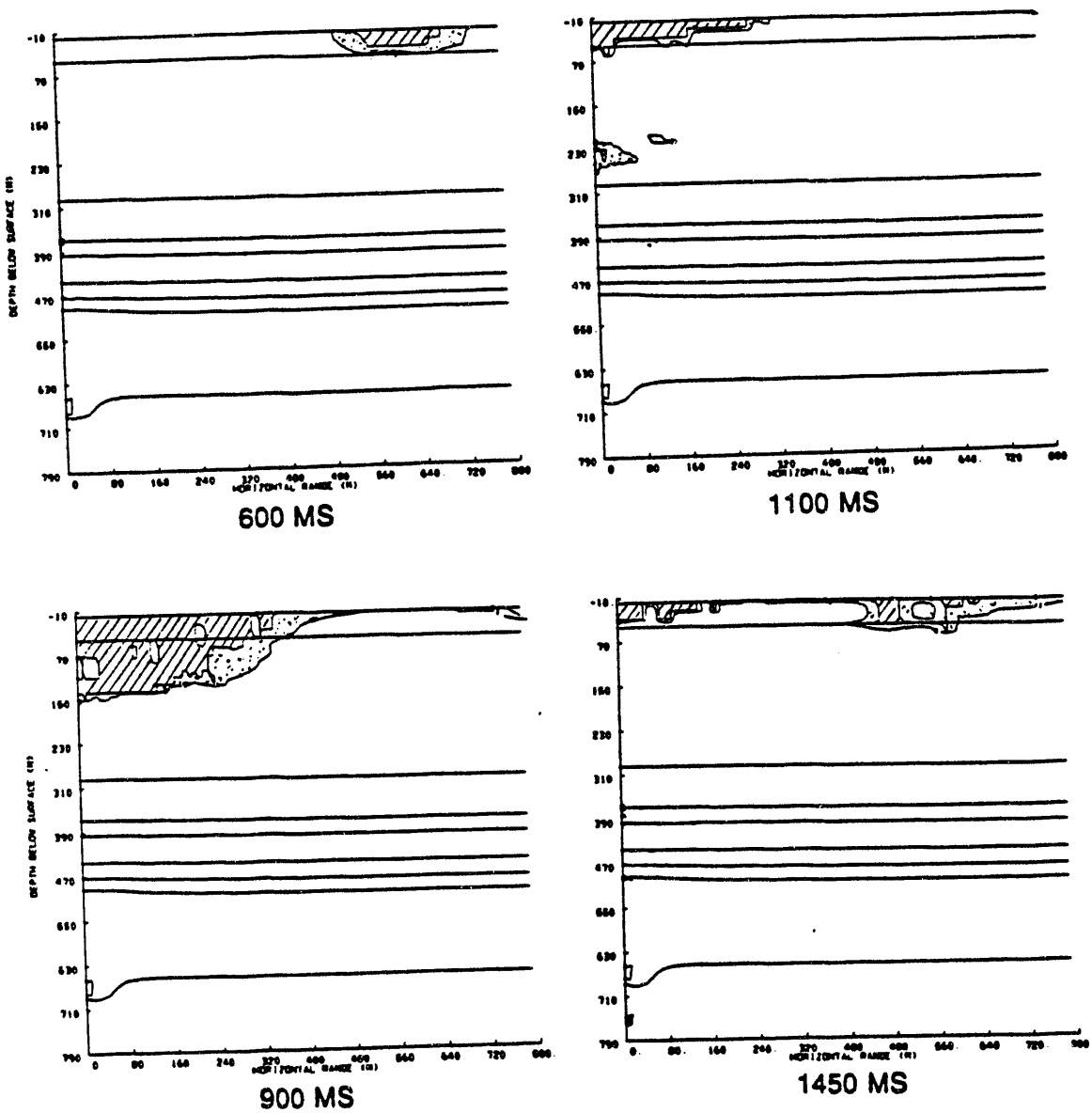

Figure 29. Evolution of spall from 600 to 1450 ms. HEARTS Case A. Regions of zero stress (spall) are hatched; regions of very low compressive stress (less than 1 MPa) are stippled.

but in different materials than for the Baseline Case. Only Station 1 is within alluvium. Because the amplitude of the stress wave is less at the tuff/alluvium interface (because of the greater range from the WP), it undergoes less failure and thus suffers less broadening within the alluvium than in the Baseline Case. On the other hand, the time of arrival and amplitude of the rebound pulse is not altered because it is a product of the WP environment, which in this case is unchanged. The net effect is that there is less time separation between the elastic precursor and the plastic peak (approximately halved) and more time separation between the plastic peak and the rebound pulse. This results in earlier spall followed by a temporary closure when the rebound pulse arrives. CAPROCK, with an alluvial thickness of 134 m, is the nearest analog to Case B. For CAPROCK, the time separation between the elastic precursor and the peak of the plastic remnant is half that of HEARTS, the same as for the calculation. However for CAPROCK the rebound pulse also is nearer the elastic precursor, unlike the calculation. These results are consistent with our modelling since we did not change the WP environment. An obvious next step is to run a case with a WP environment more like CAPROCK's. As an aside, CAPROCK had one of the highest SGZ free surface velocities ever recorded in Yucca Flat (a close second behind ATRISCO). We believe now that the high surface motion at CAPROCK is due to mutual reinforcement among the three phases.

Along the surface (Figure 31) we observe the same transition from delayed spall to an "N shape" that was observed in the Baseline Case. Figure 32 shows the velocity field at 600 ms. There is the same swirling pattern and apparent focusing along the axis of symmetry as in the Baseline Case despite the considerable differences in stratigraphy above 490 m depth. This is further evidence that the rebound is controlled primarily by the WP environment.

Figure 33 shows the evolution of spall, to be compared with Figure 25. The main difference between the Case B and the Baseline Case is the earlier spall at SGZ for Case B. The maximum kinetic energy associated with spall is 0.063 percent, 26 percent less than for the Baseline Case. The energy radiated as elastic energy from the explosion is 12 percent more than for the Baseline.

Case C - No Dense Layers (No Tmrm). The middle unit of the Tmr (Tmrm) is 80 m thick and strongly welded, providing a large impedance contrast to the other rocks in the area. The purpose here is to investigate the influence of that unit on surface motion and spall. In most parts of Yucca Flat the Tmrm is less well developed or absent. For Case C we replaced that unit by thickening the Tmrl, a non-welded unit that is weak and friable. All other properties and layering are the same as for the Baseline Case.

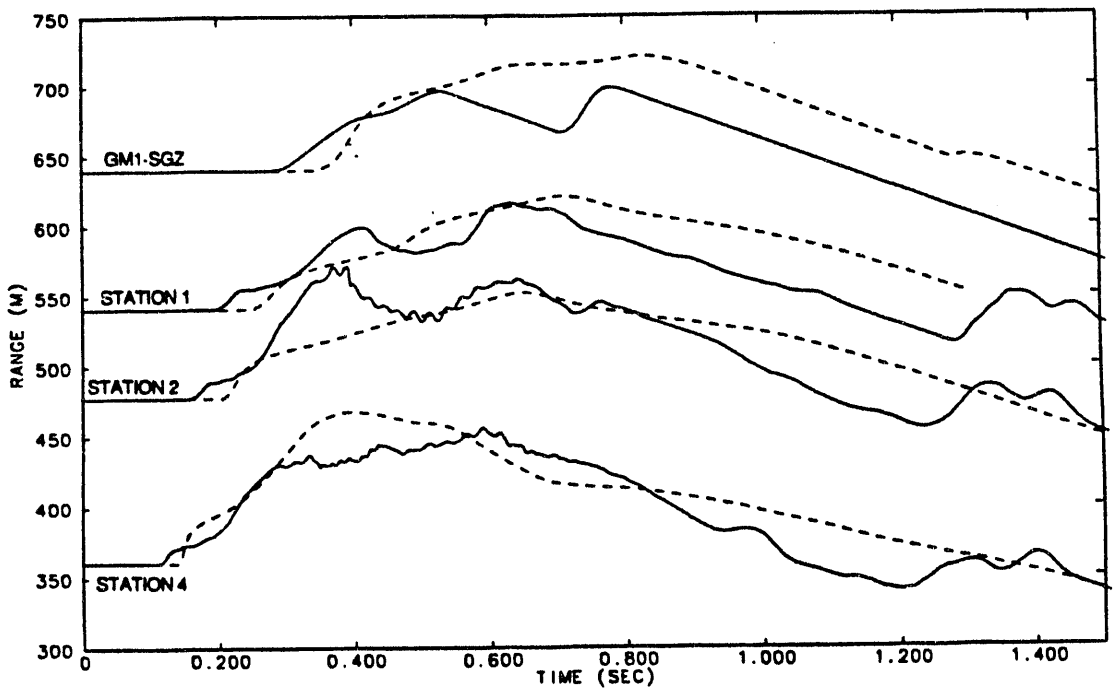

Figure 30. Comparison of calculated (solid) vs measured (dashed) vertical particle velocity waveforms from surface to 280 m depth, positioned by range from the WP. HEARTS Case B.

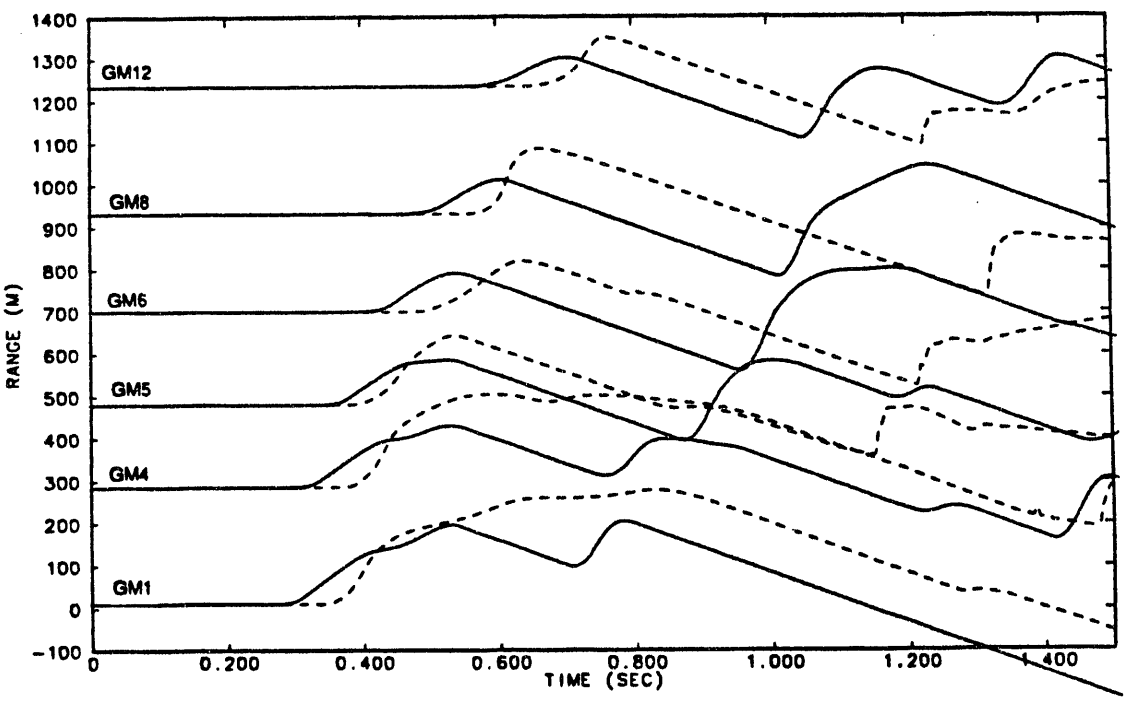

Figure 31. Comparison of calculated (solid) vs measured (dashed) vertical free surface particle velocity waveforms from SGZ to 1230 m range, positioned by range from SGZ. HEARTS Case B.

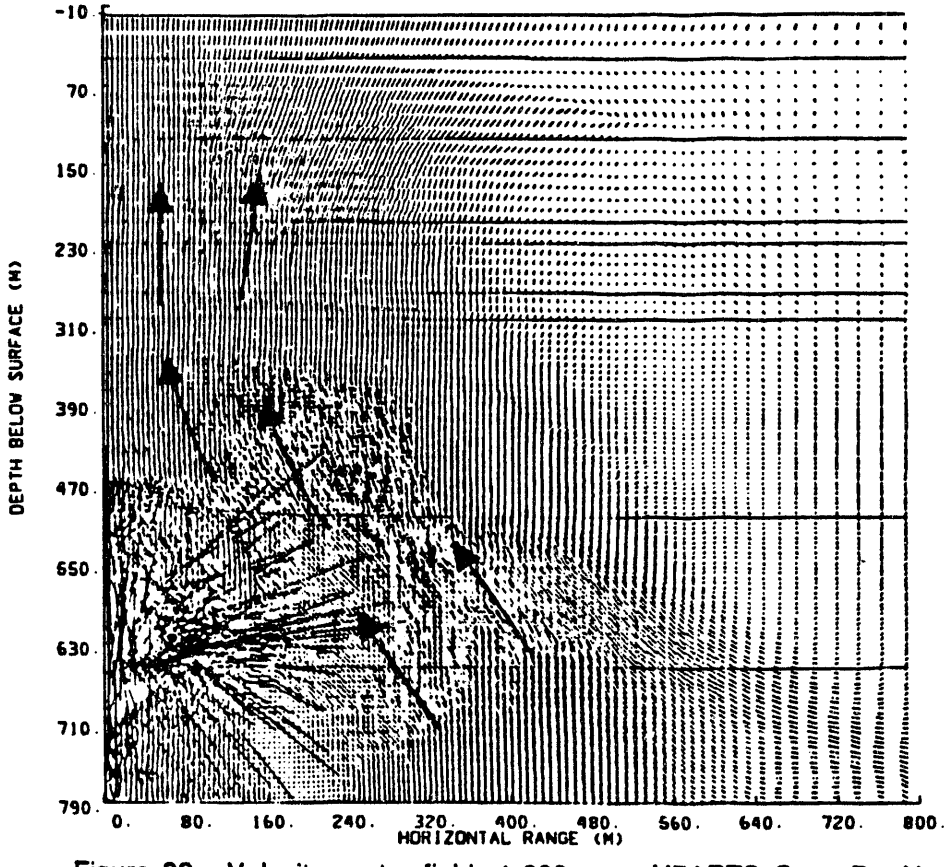

Figure 32. Velocity vector field at 600 ms. HEARTS Case B. Vector lengths are proportional to the particle velocities. Heavy arrows show general direction of flow.

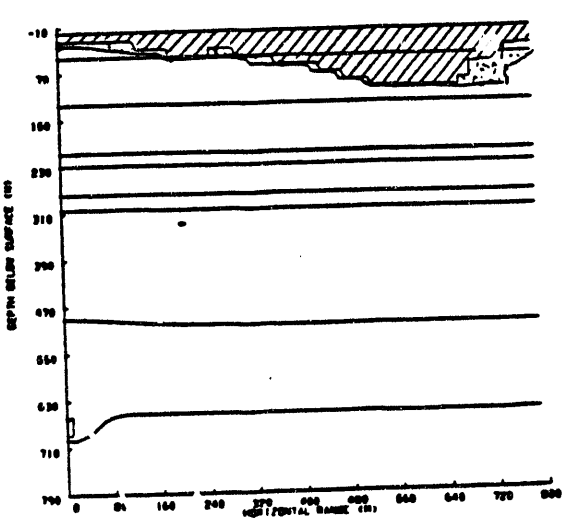

600 MS

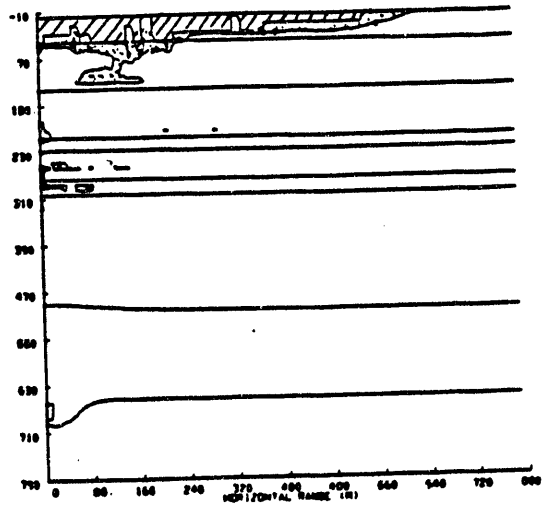

1100 MS

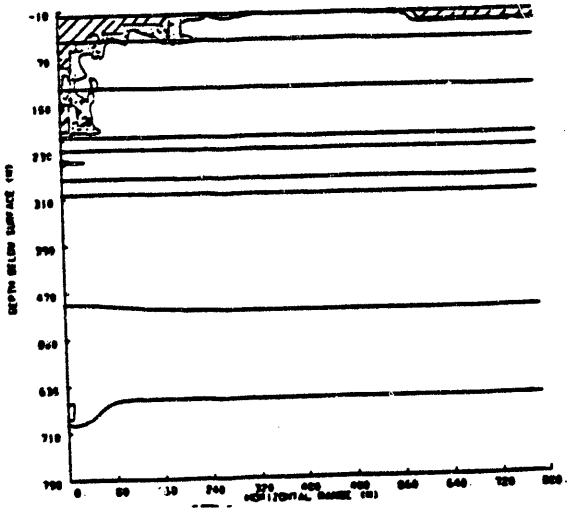

900 MS

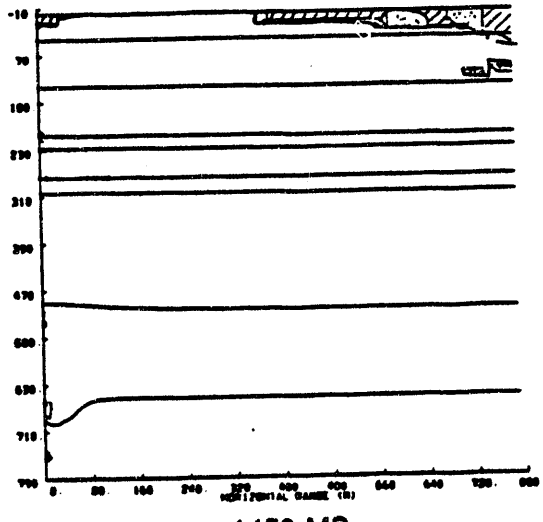

1450 MS

Figure 33. Evolution of spall from 600 to 1450 ms. HEARTS Case B. Regions of zero stress (spall) are hatched; regions of very low compressive stress (less than 1 MPa) are stippled.

Figure 34 shows the calculated vs measured waveforms in the alluvial section. In considering the amount of energy propagated to the surface there is a tradeoff between energy reflected back from a dense, strong unit (Tmrm) when that unit is present and the additional energy expended in crush and shear failure in a weaker material when the strong unit is not present. In this case, the weaker material has the greater effect. Amplitudes in the alluvium are lower and the wave is slightly broader than for the Baseline Case. Along the surface (Figure 35), the peak velocities near SGZ are lower than for the Baseline Case but at large ranges they are the same. The attenuation through the Tmrl is much less along the raypath to the more distant stations because of the greater distances (i.e., lower stress levels) involved. There is very little difference in the character of the velocity field for the two cases (Figures 36 and 22).

Figure 37 shows the evolution of spall, to be compared with Figure 25. At 1100 ms, when spall appears to be most fully developed, it is deeper beneath SGZ for Case C than for the Baseline, probably because of the longer period and therefore longer wavelength of the incident wave. Interestingly, and for reasons not entirely clear to us, the large volume of material in a "near spall" condition that developed in the Baseline Case did not develop here. The maximum kinetic energy associated with spall is 0.104 percent, 22 percent more than in the Baseline Case. The energy radiated as elastic energy from the explosion is nearly the same as the Baseline Case.

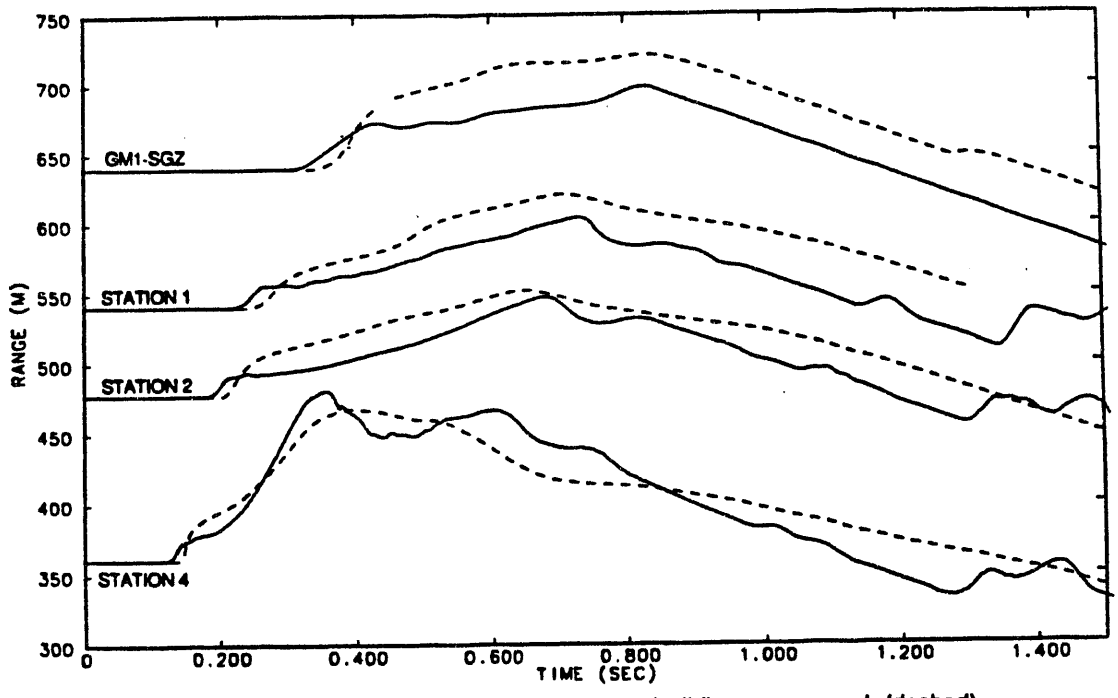

Figure 34. Comparison of calculated (solid) vs measured (dashed) vertical particle velocity waveforms from surface to 280 m depth, positioned by range from the WP. HEARTS Case C.

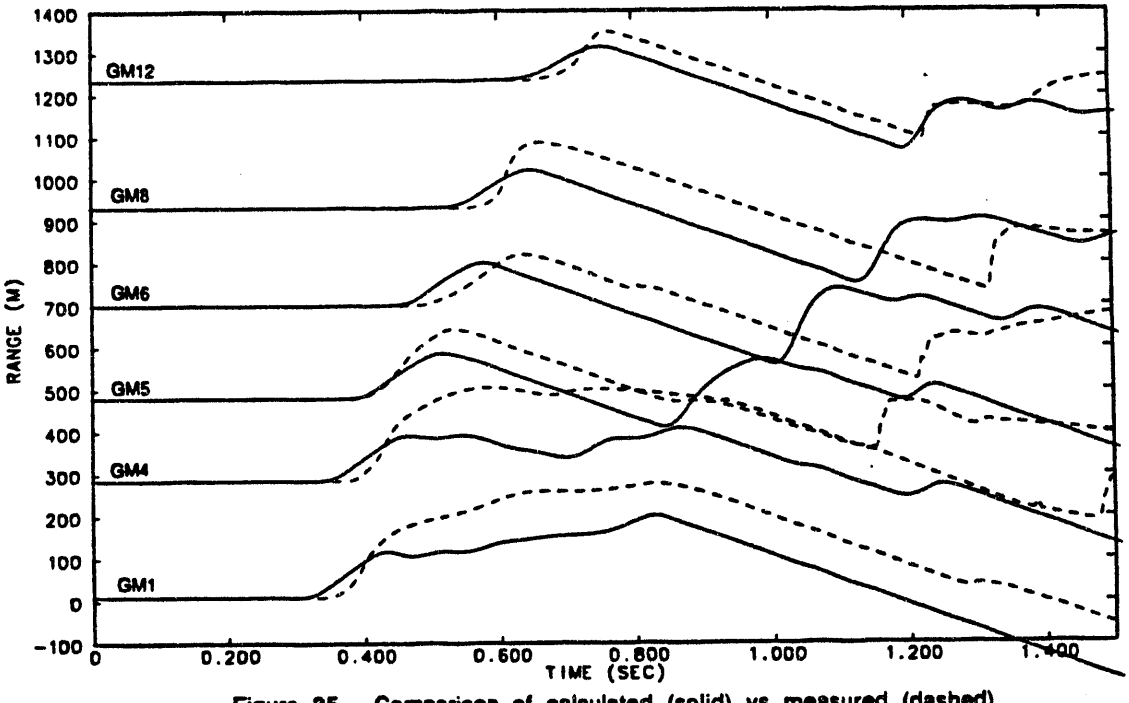

Figure 35. Comparison of calculated (solid) vs measured (dashed) vertical free surface particle velocity waveforms from SGZ to 1230 m range, positioned by range from SGZ. HEARTS Case C.

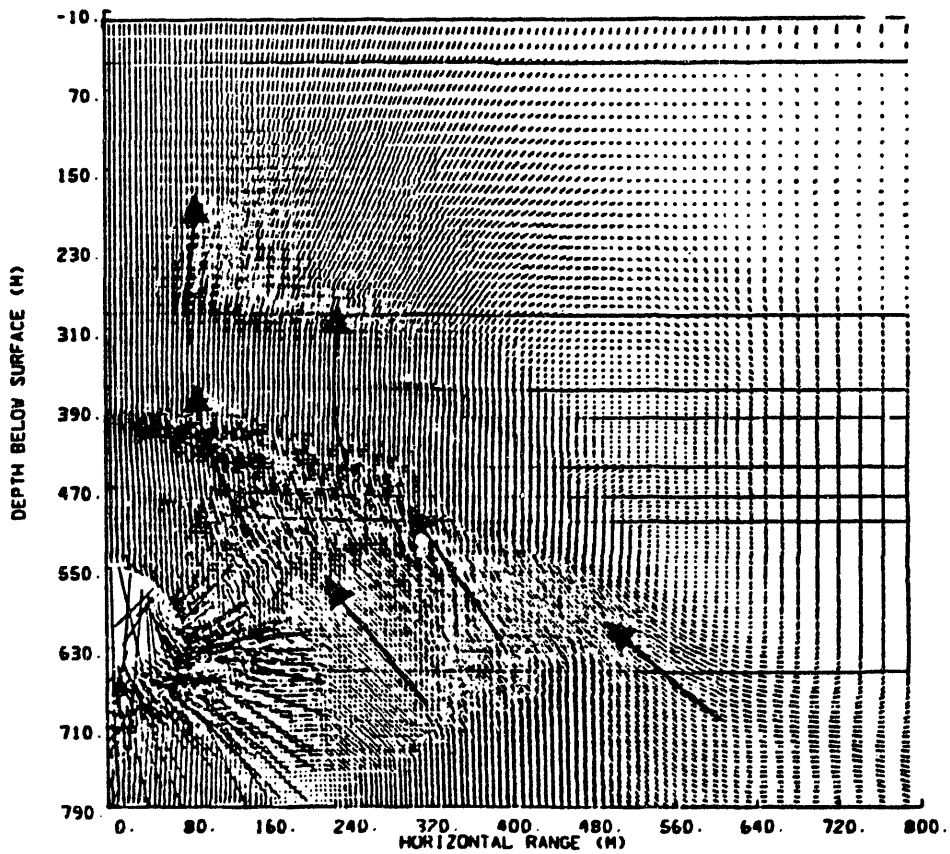

Figure 36. Velocity vector field at 600 ms. HEARTS Case C. Vector lengths are proportional to the particle velocities. Heavy arrows show general direction of flow.

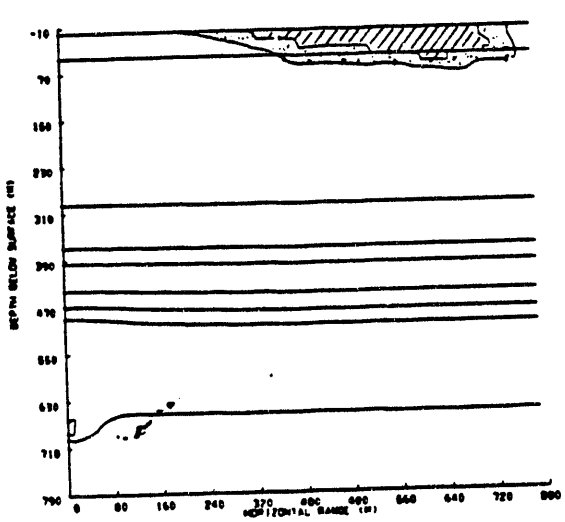

600 MS

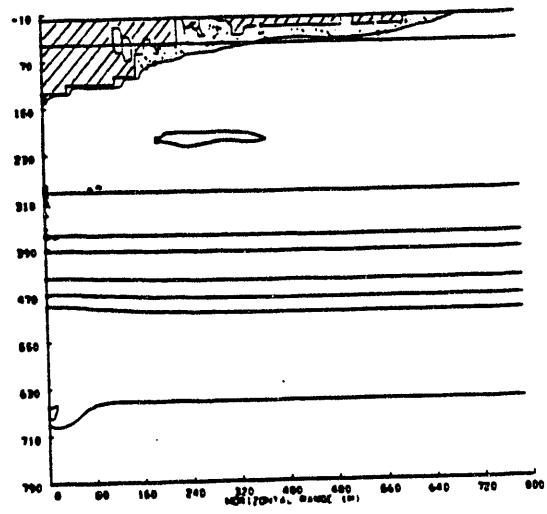

1100 MS

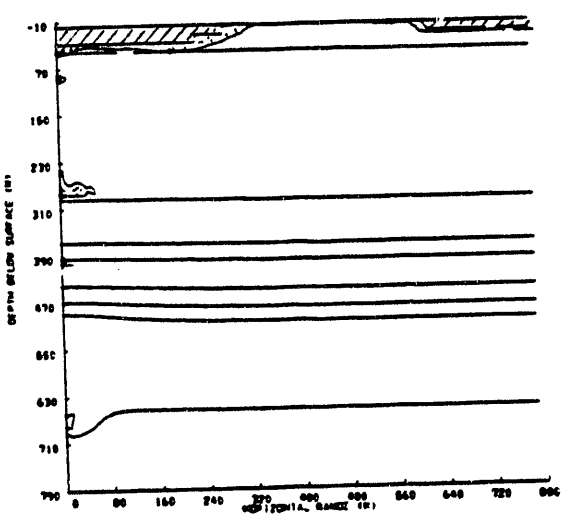

900 MS

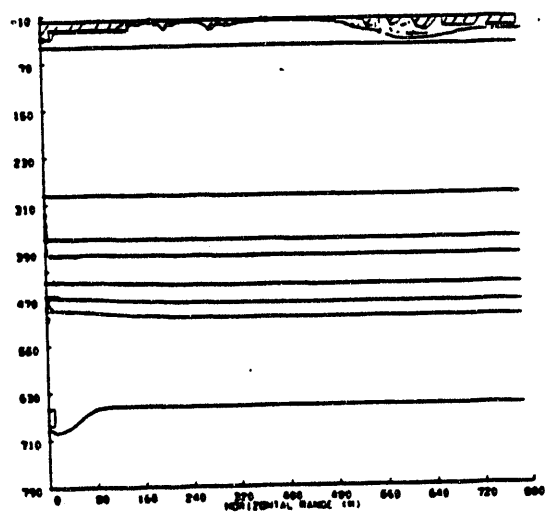

1450 MS

Figure 37. Evolution of spall from 600 to 1450 ms. HEARTS Case C. Regions of zero stress (spall) are hatched; regions of very low compressive stress (less than 1 MPa) are stippled.

TOWANDA and HOUSTON - Pahute Mesa - No Alluvial Cover.

The TOWANDA (U19ab) site geology and instrumentation are shown in Figure 38. The layering shown in the figure reflects the breakouts as they were modelled, which are controlled as much by changes in lithology as stratigraphy. This event was conducted beneath the water table at a depth of 660 m. The stratigraphic sequence at the U19ab site is comprised of an interlayering of lavas, welded tuffs and non-welded tuffs. The WP is in non-welded tuff. At the surface, the uppermost 15 m is low density Ammonia Tanks Tuff (Tma). Below that, extending to a depth of 310 m, is the Rainier Mesa Tuff (Tmr) which generally is much thicker on Pahute Mesa than in Yucca Flat. It is a dense, moderately to strongly welded ash flow tuff that is of special interest in this study because it lies within the region of spall for both TOWANDA and HOUSTON. An extensive array of measurements were attempted in two satellite holes as well as in the emplacement hole. Sandia National Laboratory fielded some deep stress and motion gages and Los Alamos fielded both deep and shallow accelerometers in one of the satellite holes as well as in the emplacement hole. All deep gages terminated early, i.e., before reaching the first particle velocity peak. The deepest gage station to survive long enough to reach peak particle velocity was MH-B located in the emplacement hole at 440 m. The deepest satellite hole gage to reach the velocity peak was located at 305 m depth (SAT-2G), less than one-half DOB. From 305 m to SGZ there are eight stations, all of which did survive. Only those locations with gages that survived long enough to be useful to our analysis are shown in the figure. As far as we know, these near surface measurements provide a more detailed picture of subsurface spall on Pahute Mesa than for any other event. Table II describes in more detail the stratigraphy at the TOWANDA site as it was used in the modelling along with values of bulk density, gas filled porosity and qualitative descriptions of the compressibilities and shear strengths.

Figure 39 shows the site geology and the subsurface and surface motion station locations for HOUSTON (U19az). This event was conducted in tuff above the water table at a depth of 595 m, and a scaled-depth-of-burial similar to that for TOWANDA. The WP was in densely welded tuff. The near surface materials are comprised of a 25 m thick moderately welded caprock underlain by 40 m of non-welded ash flow tuff, both belonging to the Tma stratigraphic unit. Below the Tma, extending to a depth of 255 m, is the moderately to densely welded Tmr. Unlike MERLIN, HEARTS and TOWANDA, all subsurface accelerometer stations were in the emplacement hole; there were no satellite/instrument holes for HOUSTON. The instruments were fielded by Los Alamos. The gages at all five depths survived ground shock and recorded motion well past the first particle velocity peak. In fact, four of the five (A, C, E and F) survived to maximum recording time of seven seconds. How well the motion from such measurements represents the free field

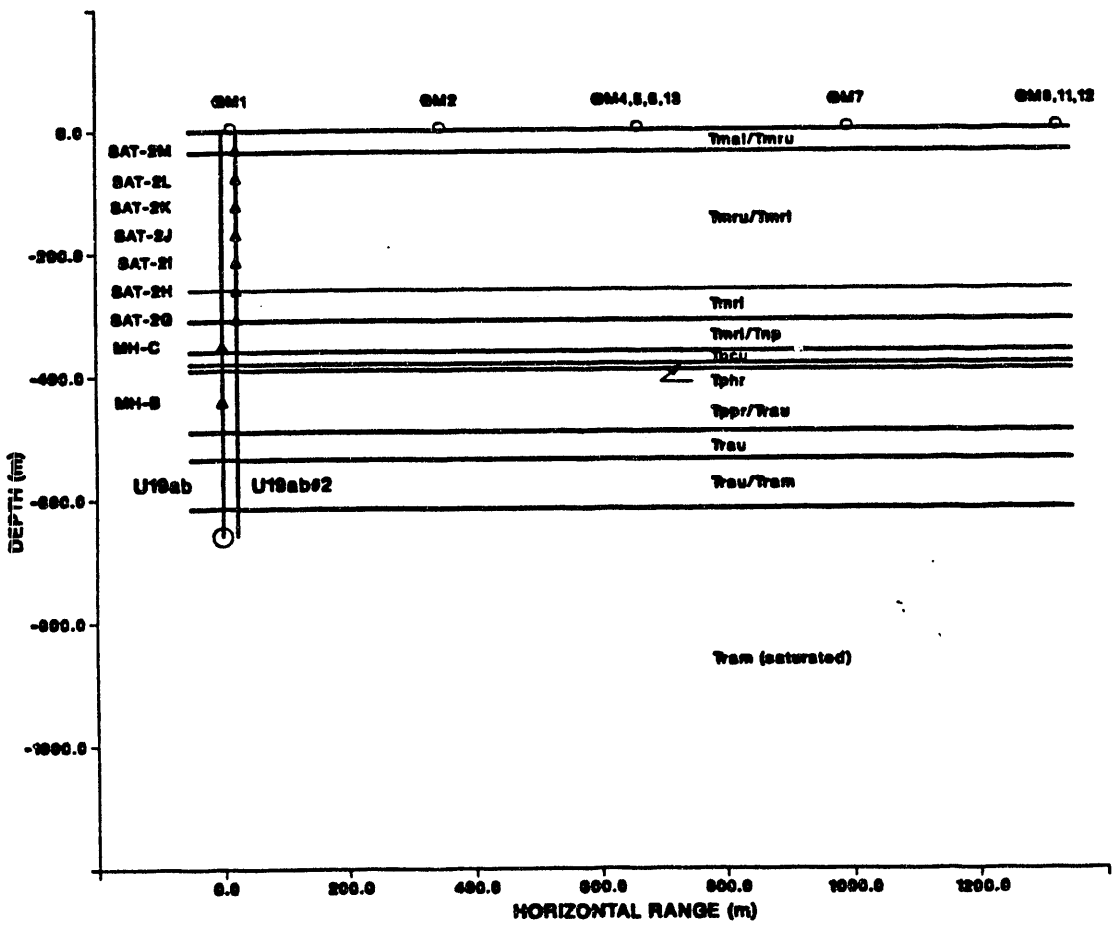

Figure 38. TOWANDA ground motion station locations and stratigraphic section as it was modelled in the Baseline Case. Triangles represent subsurface vertical accelerometer stations. Circles represent three component surface accelerometer stations.

Table II

Modelled Stratigraphy at U19ab - TOWANDA

Unit	Depths (m)	Description (rho=bulk density in Mg/m^3, GFP=gas porosity in percent)
Tmal/ Tmru	0-35	15 m of Ammonia Tanks Tuff; 20 m of upper Rainier Mesa Tuff- ash flow tuffs - non-welded to moderately welded; rho=1.67; GFP=17; moderately compressible; moderate shear strength; very low sound speed.
Tmru/ Tmrl	35-260	29 m of Upper Rainier Mesa Tuff, 196 m of Lower Rainier Mesa Tuff - ash flow tuff - partially to moderately welded; rho=2.2; GFP=6.8; stiff in compression; very high shear strength.
Tmrl	260-310	Lower Rainier Mesa Tuff - ash flow tuff - vitrophyric; rho=2.3; GFP=0.8; very stiff in compression; high shear strength; high sound speed.
Tmrl/ Tnp	310-360	24 m of Lower Rainier Mesa Tuff; 26 m of Pool Unit - ash flow and reworked tuff - non-welded; rho=1.8; GFP=22.7; moderately compressible; low shear strength.
Tpcu	360-380	Tiva Canyon Tuff - ash flow tuff - vitrophyric; rho=2.2; GFP=5; stiff in compression; very high shear strength.
Tphr	380-390	Non-welded tuff - vitric; rho=1.48; GFP=27; moderate compressibility; low shear strength.
Tppr/ Trau	390-490	Upper 79 m vitric, in places frothy lava - lower 21 m vitric, non-welded tuff; rho=1.9; GFP=18.9; Stiff in compression; moderate shear strength.
Trau	490-535	Non-welded tuff - zeolitic; rho=2.15; GFP=7.2; moderate compressibility; moderate shear strength.
Trau/ Tram	535-615	Non-welded tuff - zeolitic; rho=2.15; GFP=7.2; stiff; relatively high shear strength; water table at 615 m.
Tram	615-Base	Non-welded tuff - zeolitic; rho=2.41; GFP=0; stiff because saturated; relatively high shear strength.

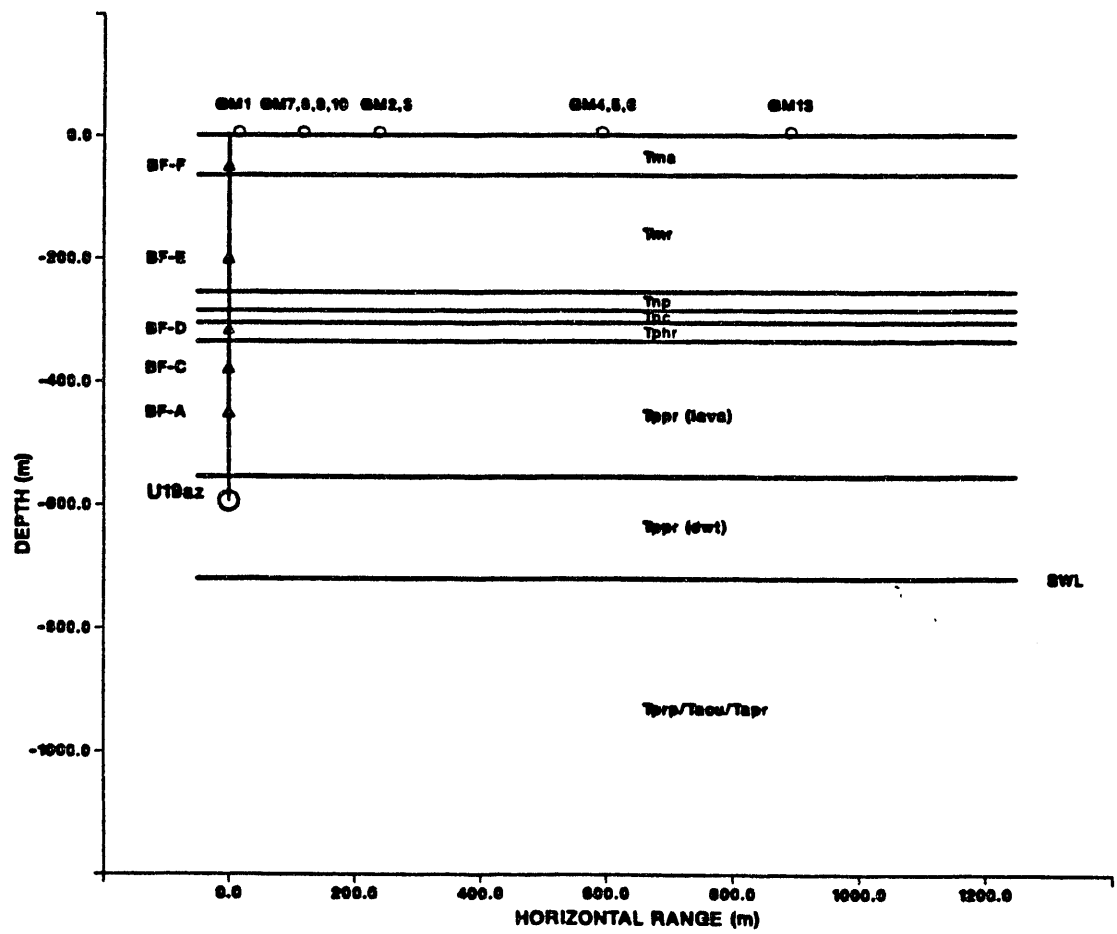

Figure 39. HOUSTON ground motion station locations and the stratigraphic section as it was modelled in the calculation. Triangles represent subsurface vertical accelerometer stations. Circles represent three component surface accelerometer stations.

Table III

Modelled Stratigraphy at U19az - HOUSTON

Unit	Depths (m)	Description (rho=bulk density in Mg/m^3, GFP=gas porosity in percent)
Tma/ Tmr	0 - 65	Upper 40 m is Ammonia Tanks Tuff - non-welded to partially-welded to bedded; lower 25 m is Rainier Mesa Tuff - bedded; rho=1.6; GFP=24; highly compressible; low shear strength.
Tmr	65-255	Rainier Mesa Tuff - partially to densely welded; rho=2.16; GFP=8.5; stiff in compression; high shear strength.
Tnp	255-285	Pool Unit - non-welded tuff; rho=1.6; GFP=21; moderately compressible; low shear strength.
Tpc	285-305	Tiva Canyon Tuff - moderately to densely welded to vitrophyric; rho=2.18; GFP=5.8; very stiff in compression; very high shear strength.
Tphr	305-335	Bedded Tuff; rho=1.6; GFP=21; moderately compressible; low shear strength.
Tppr	335-555	Lava; increases with depth from rho=1.78 at top to 2.28 at base; GFP=23 at top to 1.6 at base; stiff at top to very stiff at base; moderate shear strength at top to high shear strength at base.
Tppr	555-720	Densely welded tuff; rho=2.39; GFP=1.3; very stiff in compression; high shear strength. Water table at 720 m.
Tprp	720-Base	Rhyolite of Silent Canyon and older units; rho=2.41; GFP=0; very stiff in compression; high shear strength.

motion has not been firmly established. Based on the few comparisons made between emplacement and satellite hole measurements at the NTS, including TOWANDA, and also on (unreported) computer simulations, we believe the general shape and breadth of the waveforms are representative of the free field; however the early part of the rise probably lags the free field due to compaction of stemming materials. Table III describes in more detail the stratigraphy as it was used in the modelling along with values of bulk density, gas filled porosity and qualitative descriptions of the compressibilities and shear strengths.

An important point is that the stratigraphy at the two sites is similar down to and including the Tnp, Tpe, Tphr sequence. Below that the two settings are quite dissimilar. The deeper units at HOUSTON are dense lavas and dense, strongly welded tuffs. At TOWANDA the lavas are of relatively low density and the tuffs are non-welded.

Figure 40 shows the accelerometer measurements from the TOWANDA satellite hole from 305 m to the surface. Superposed on the plot are straight line segments drawn connecting 1) first detectable motion and 2) the peak acceleration of a downward propagating rarefaction. Similar to the construction of Figure 18, line 2 connects the intersection points of picked times and station ranges. Between Stations 2G and 2H, the apparent elastic wave propagation velocity is about 4000 m/s. This interval is comprised of a very high density (~2.3 Mg/m3) portion of the Tmr, including a vitrophyre. Between Stations 2H and 2K, the velocity is relatively constant at 2100 m/s. This comprises a major portion of the Tmr, and there are no vitrophyric sections present. Between 2K and 2L, still within the Tmr, the velocity drops to about 1800 m/s. In the uppermost interval, between 2L and the surface, the apparent velocity is only 650 m/s. The interval includes the remaining 15 m of Tmr plus the Tma. This velocity structure is the key to the picture of subsurface spall that develops for TOWANDA.

At the four deepest stations the shape and the width of the first positive acceleration phase are very similar, suggesting that the wave is elastic or nearly elastic. Above that point there is interference from the rarefaction so one cannot be certain. The apparent propagation velocity of the rarefaction (line 2) between 2K and 2H appears to be a bit higher than the elastic propagation velocity inferred from the first arrivals over the same interval. The rarefaction identified by line 2 is not generated at the free surface but rather at a subsurface impedance discontinuity. By projecting the rarefaction back to an origin point and using apparent velocities from the first arrivals (line 1) we estimate that the impedance change occurs at a depth of about 35 m. Density logs and geophone surveys at the site are not very consistent in locating an impedance discontinuity at this depth, nor is there a change in stratigraphy as currently interpreted, but a large impedance change surely must exist. The substantial (80 percent) amplitude increase observed at Station 2M is caused by this

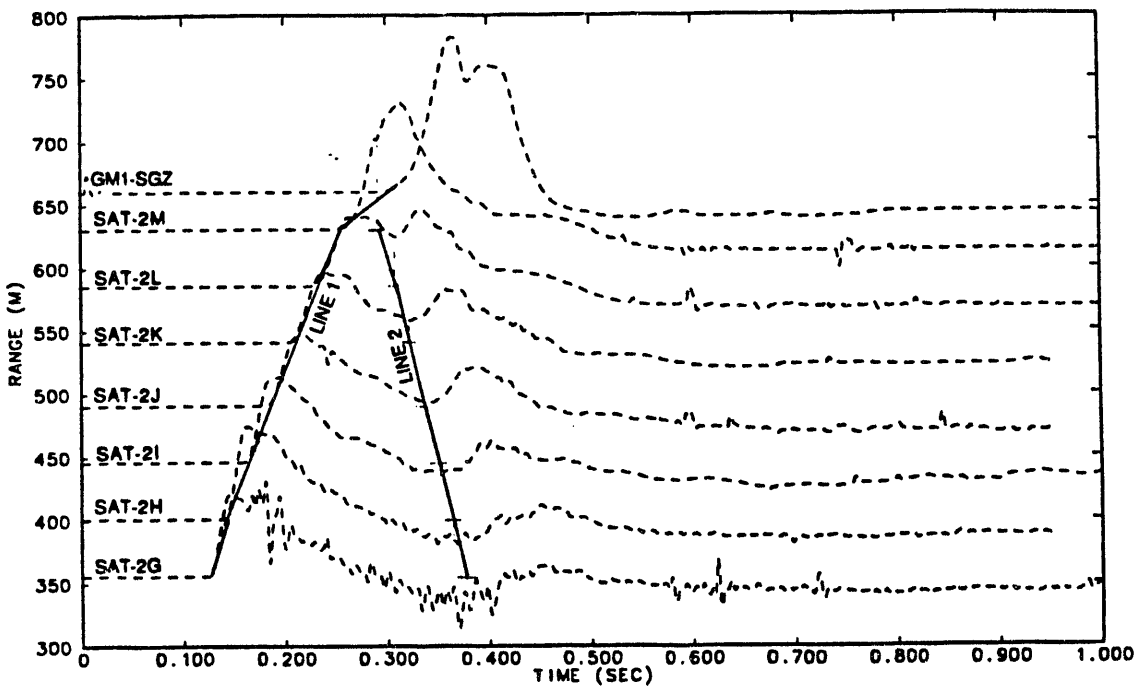

Figure 40. Measured vertical acceleration waveforms from the surface to 305 m depth, positioned by range from the WP. TOWANDA event. Line 1 tracks the first arrivals; line 2 tracks a downward propagating rarefaction.

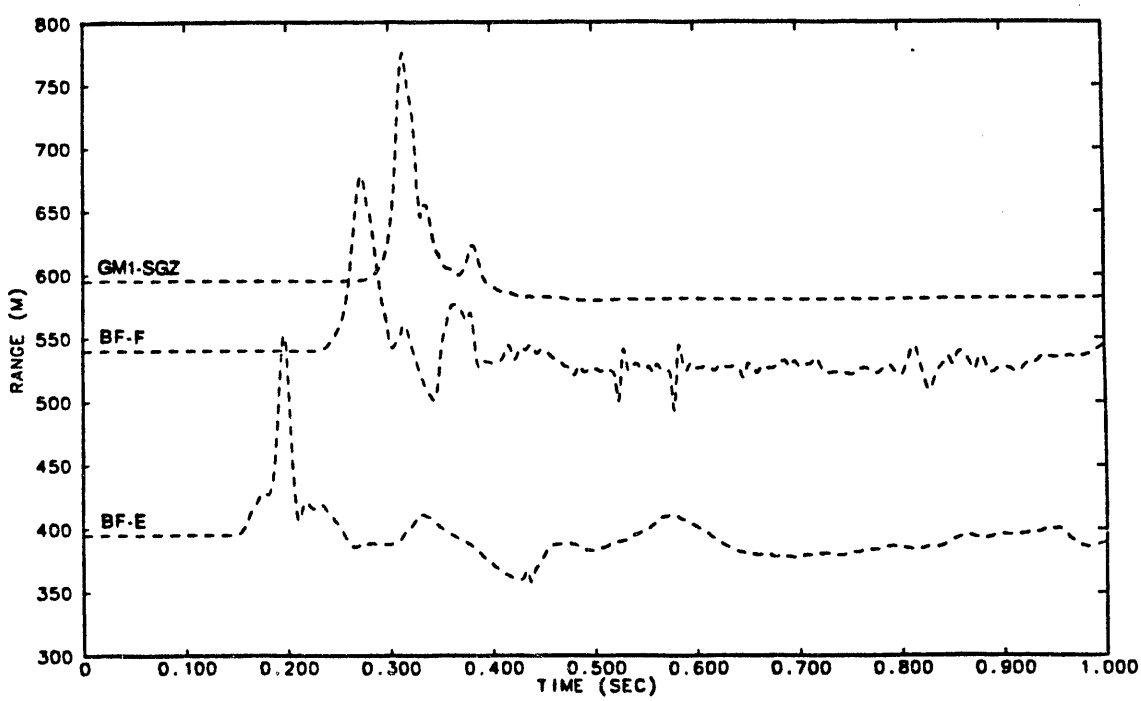

Figure 41. Measured vertical accelerometer waveforms from surface to 200 m depth, positioned by range from the WP. HOUSTON event.

impedance break, not the free surface. There is a very broad, gradual decay toward the negative 1 g spall acceleration in all of the waveforms. However they do not all actually reach negative 1 g. Furthermore, the deeper measurements terminated early so we cannot use a spall closure signature as evidence of whether they did or did not spall. It is not entirely clear what the true "depth of spall" is for TOWANDA. Patton (1990) estimates a depth of 280 m from his analysis. The overall effect of the near surface low velocity layer is to broaden the effective wavelength of the rarefaction and deepen spall.

Figure 41 is a plot similar to Figure 40 but for the HOUSTON event. Again the waveforms are only from stations in the Tmr on up. The amplitude and time scales are the same in both figures. For HOUSTON, the waveforms are much more impulsive with higher peak amplitudes and shorter periods. The surface generated rarefaction appears to be at least partly responsible for the positive excursion at 0.36 sec at BF-F. From the first arrivals, there is no indication of a substantial near surface velocity change at HOUSTON. Spall appears to be much shallower for HOUSTON than for TOWANDA. The rock spalls at 50 m depth but there is no indication of spall at 200 m depth.

Figures 42 and 43 are the integrations (particle velocities) of the accelerometer waveforms of Figures 40 and 41. The time and particle velocity amplitude scales are the same. The amplitudes are considerably higher for TOWANDA because of the broader acceleration pulse. Figure 44 compares SGZ motions for both events to 3 sec, past spall closure. The ground motion was substantially greater at TOWANDA despite that event's greater SDOB, however such differences are not particularly unusual for Pahute Mesa. It is our goal to understand the differences.

Figure 45 shows a comparison of a subset of the Figure 42 TOWANDA waveforms with a calculation that includes a velocity discontinuity at 35 m. The surface arrival is too early in the calculation so the separation between rarefactions from the 35 m discontinuity and the free surface is not as distinct as in the measurements. In this instance, some interfering numerical noise also is generated at the subsurface interface that propagates down with the rarefaction. Along the free surface (Figure 46) the calculations do not capture the first arrival times, spall closure times or the attenuation of amplitude with range. The calculated first arrivals lead the measurements by as much as 200 ms at the farther-out stations. There is a geologic/topographic explanation for this. The TOWANDA emplacement hole is sited in a depression surrounded on all sides by hills. The Tma is interpreted by geologists to be thinnest beneath SGZ, rapidly thickening away from SGZ. This lateral change in thickness probably is responsible for most of the differences between calculations and measurements along the free surface. There has been no attempt to model the lateral variation although in this particular instance it is possible to do a first order approximation of the effect using our two-dimensional, axisymmetric modelling. With a few minor adjustments in the near

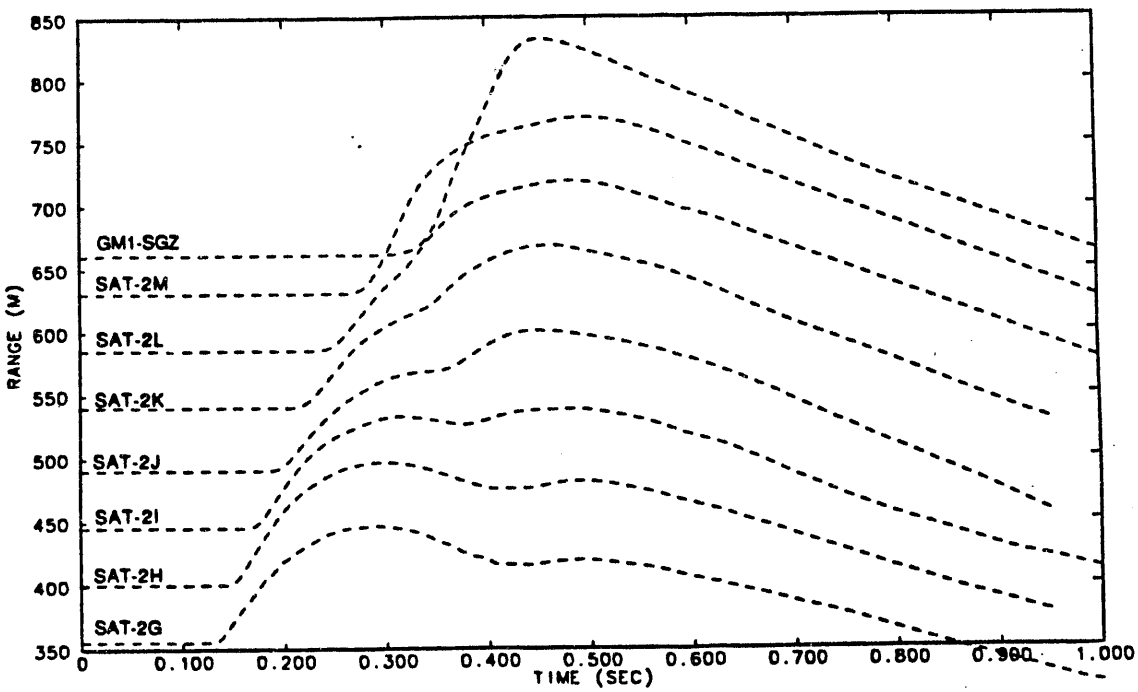

Figure 42. Measured vertical particle velocity waveforms from the surface to 305 m depth, positioned by range from the WP. TOWANDA event.

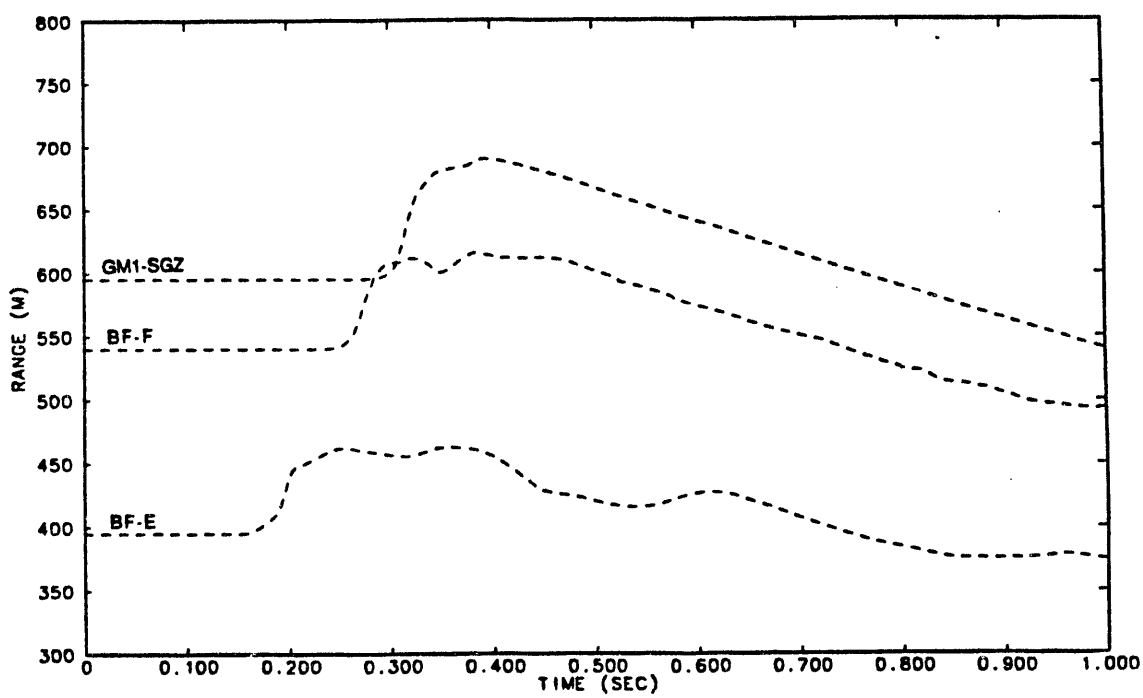

Figure 43. Measured vertical particle velocity waveforms from surface to 200 m depth, positioned by range from the WP. HOUSTON event.

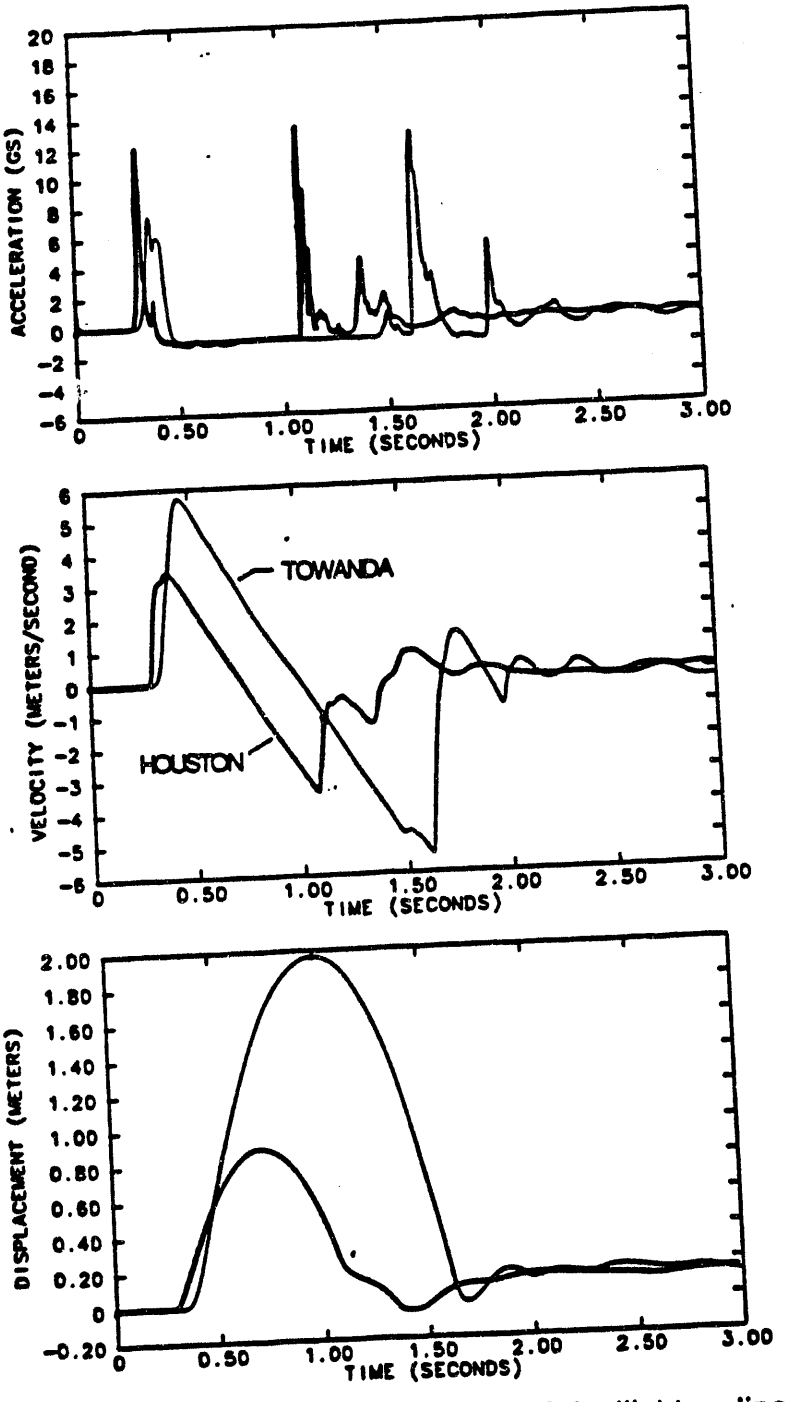

Figure 44. Comparison of TOWANDA (lighter line) and HOUSTON (heavier line) SGZ vertical free surface acceleration, velocity and displacement waveforms to 3 sec.

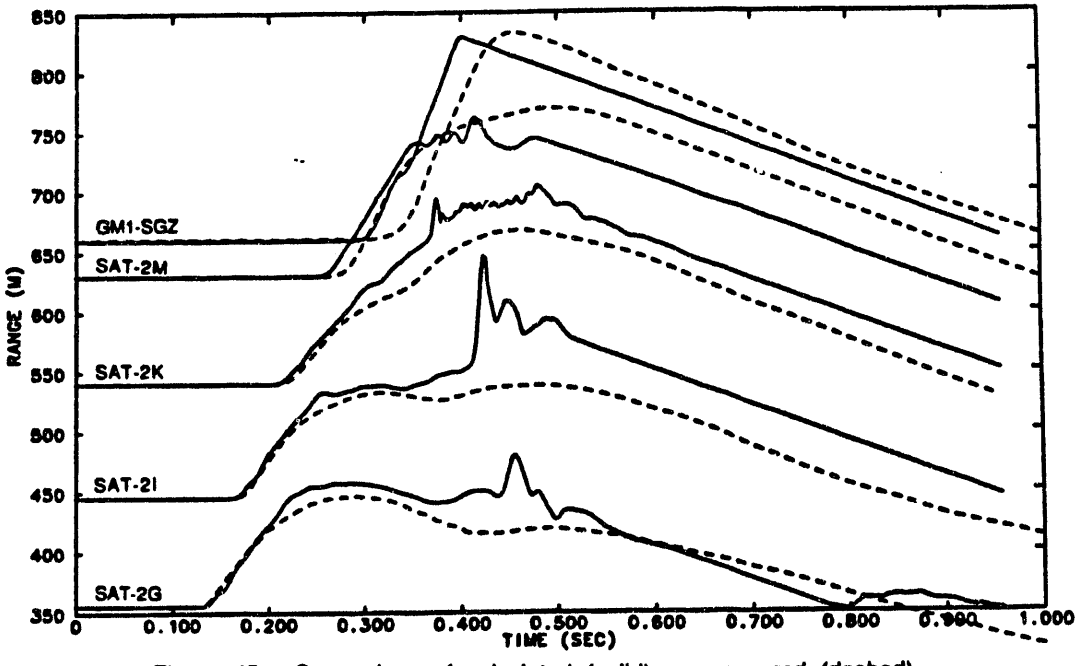

Figure 45. Comparison of calculated (solid) vs measured (dashed) vertical particle velocity waveforms from surface to 305 m depth, positioned by range from the WP. TOWANDA Baseline Case.

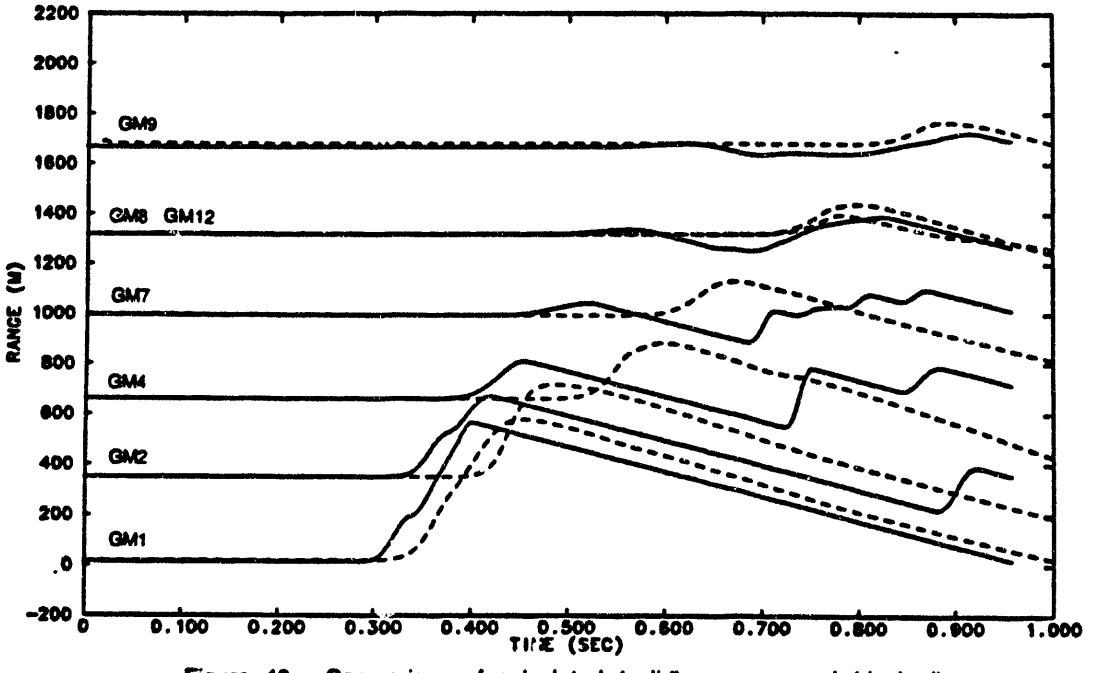

Figure 46. Comparison of calculated (solid) vs measured (dashed) vertical free surface particle velocity waveforms from SGZ to 1635 m range, positioned by range from SGZ. TOWANDA Baseline Case.

surface layering, we believe we have a Baseline Case for future TOWANDA spall parameter studies.

Figure 47 shows the development of spall in the TOWANDA calculation. Directly beneath SGZ, spall reaches the base of the Tmr (310 m) by 600 ms. Spall is confined to the (unrealistically) thin Tma away from SGZ which causes the reduced amplitudes and premature spall closures noted in connection with Figure 46. The deep spall beneath SGZ is consistent with the measurements. Figure 48 shows the velocity field at 600 ms. Compared to HEARTS, the motions appear to be more locally controlled and below about 350 m are directed downward. There is no indication of a rebound pulse propagating toward the surface either in the measurements or calculation. The maximum spall associated kinetic energy is 0.160 percent. The total energy radiated as elastic waves from the point source explosion is 0.596 percent, so the energy potentially available from the spall zone as a secondary source for seismic waves is about one-quarter that available from the point source explosion itself. Both the calculated energy available for seismic wave propagation and the spall energy are quite a bit lower than those estimated by Patton (1990) for Pahute Mesa events in general, but interestingly he concluded that about one quarter of the available energy outside the non-linear region goes into spall, similar to our conclusion.

With regard to the analysis of surface motion, the HOUSTON calculations have been largely unfruitful to this point in the study. We have no calculation in which we have sufficient confidence to consider it a Baseline Case for parameter studies. Figure 49 compares subsurface particle velocities from our best calculation so far with the subsurface measurements. Figure 50 compares free surface waveforms. Although we do quite well in matching the free surface motions for as far as the calculation was carried in time, we suspect that our modelling of subsurface spall is incorrect. Of concern is the disagreement at Station BF-E between measured and calculated waveforms after 270 ms.

Elements of the measured waveforms that we are replicating are initial risetimes and first-peak amplitudes, which are quite different (more impulsive) than those for TOWANDA. This probably is responsible for the good early agreement at the free surface where spall is initiated before the later phases can have an effect. The more impulsive nature of the HOUSTON data was discussed above and we are capturing that in the calculation. The differences between the HOUSTON and TOWANDA motions stem from differences in relative locations of the WP's to the water table and the rock properties within a few cavity radii. Because HOUSTON is above the water table, shock coupling of energy into the rock is relatively weak. Away from the WP the high strength of the rock retards broadening of the wave. These effects combine to create the relatively low amplitude, narrow pulse observed for HOUSTON. Because TOWANDA is beneath the water table, there is strong

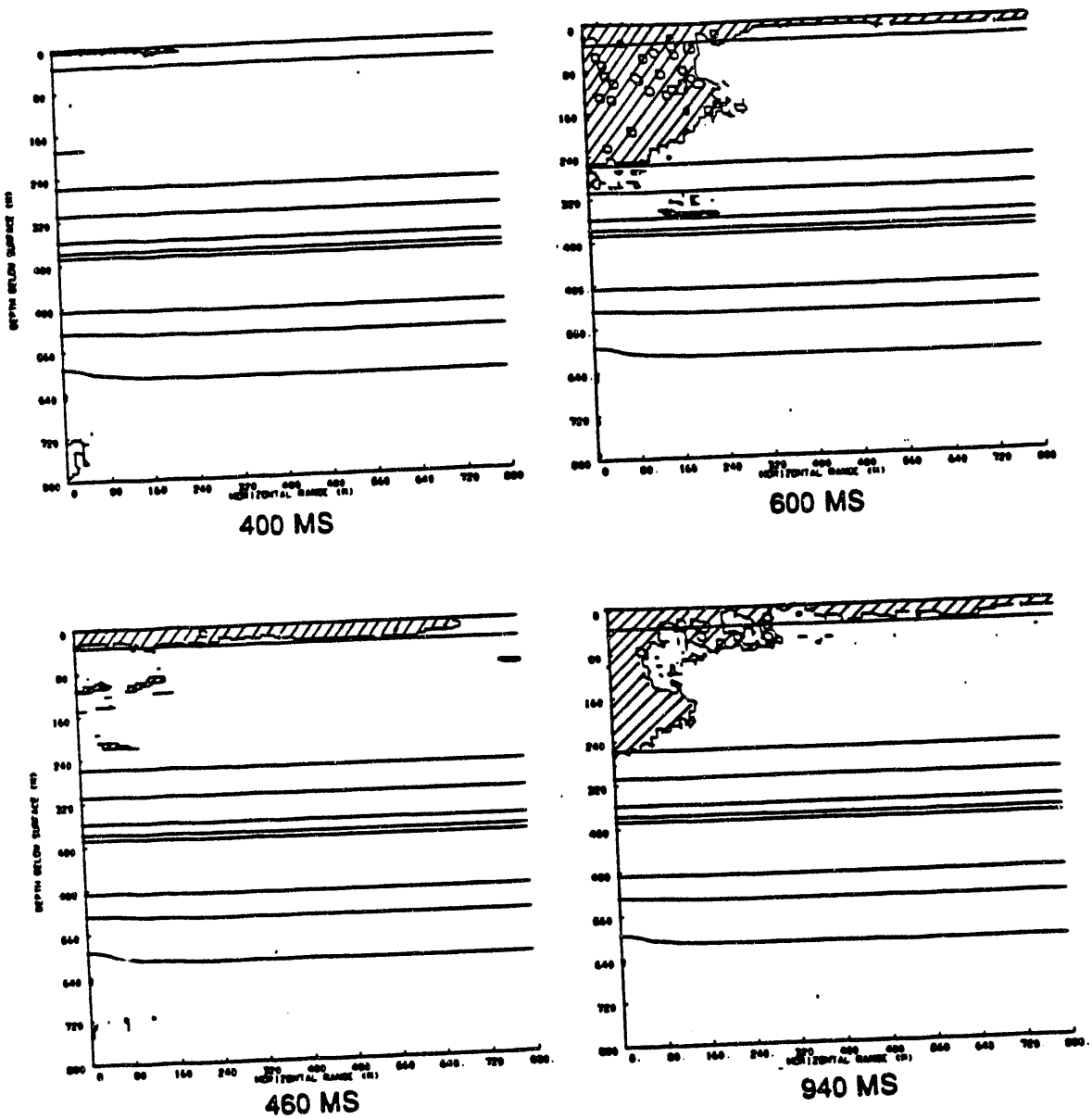

Figure 47. Evolution of spall from 400 to 940 ms. TOWANDA Baseline Case. Regions of zero stress (spall) are hatched.

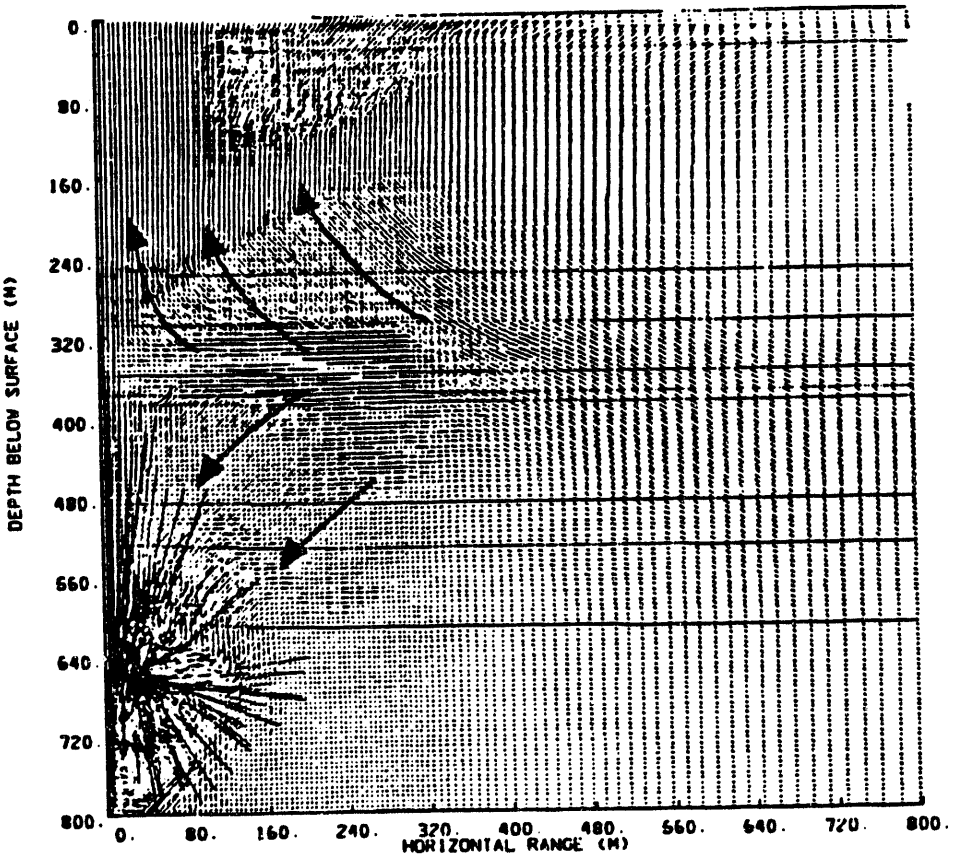

Figure 48. Velocity vector field at 600 ms. TOWANDA Baseline Case. Vector lengths are proportional to the particle velocities. Heavy arrows show general direction of flow.

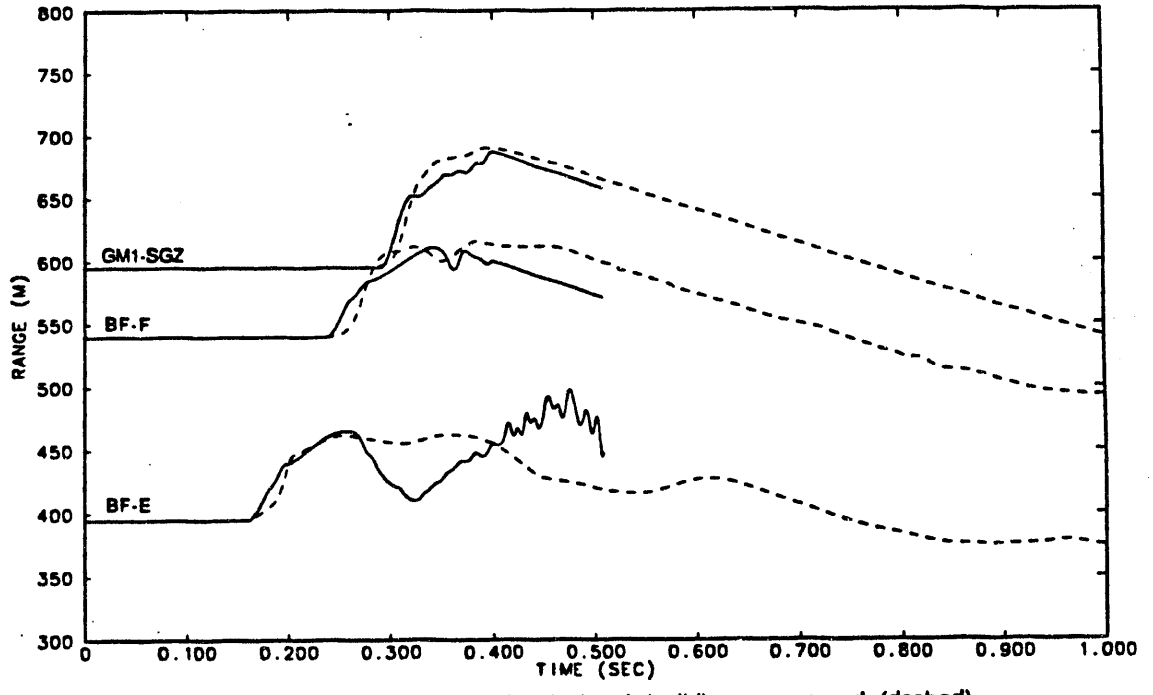

Figure 49. Comparison of calculated (solid) vs measured (dashed) vertical particle velocity waveforms from surface to 200 m depth, positioned by range from the WP. HOUSTON calculation.

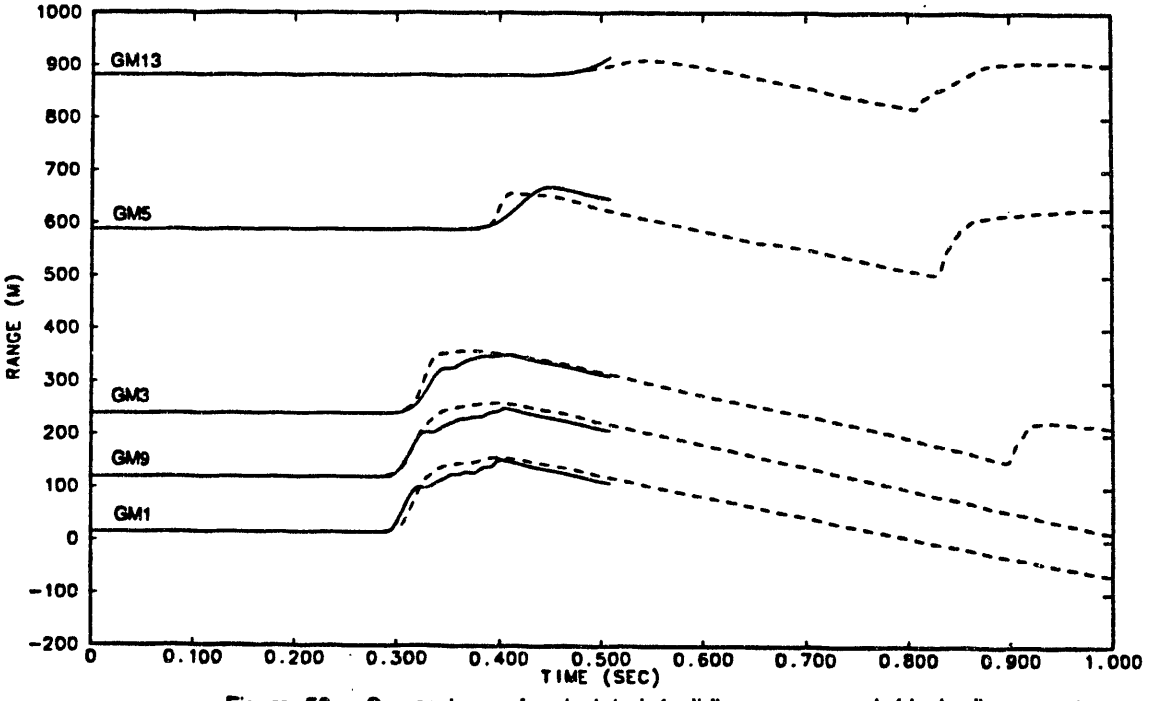

Figure 50. Comparison of calculated (solid) vs measured (dashed) vertical free surface particle velocity waveforms from SGZ to 890 m range, positioned by range from SGZ. HOUSTON calculation.

shock coupling. However, the rocks above the water table out to a few cavity radii are generally more compressible and weaker in shear, causing a broadening of the wave. These effects combine to form the broad, high amplitude pulse observed for TOWANDA. What is observed in the upper part of the section and at the surface is largely determined by what happened deep.

No parameter studies are being reported for either TOWANDA or HOUSTON, but such studies are in progress for TOWANDA.

IV. SUMMARY AND CONCLUSIONS

While the study is incomplete, we feel that we have added to the body of understanding regarding surface motion and spall from underground nuclear tests. Following, we summarize what we consider to be the more important and interesting findings.

For MERLIN we have offered a plausible explanation for the less than negative 1 g "spall" accelerations so often observed on low yield events conducted in alluvium. We believe it is associated with a shear failure phenomenon as the incident wave is reflected at the free surface. Surface motion and spall are sensitive to relatively small changes in the crush and shear strength of the alluvium. The energy associated with spall, and potentially available as a secondary source for seismic waves, appears to be directly proportional to the yield and is insensitive to depth of burial, despite differences in the distribution of the spalled mass. The energy potentially available for seismic wave generation from spall closure in alluvium is about one-tenth of that available directly from the point source explosion.

For HEARTS (and presumably for other events conducted beneath the water table in Yucca Flat) we have established a plausible mechanism leading to delayed spall and amplification of the peak free surface velocity near SGZ. We identify three phases important to surface motion, two of which were well known before the study and one that was not. These are the elastic precursor, the remnant of the plastic wave and a rebound pulse that originates deep in the section. The relative contribution of the plastic remnant is a strong function of range to the tuff/alluvium interface. The amplitude and timing of the rebound pulse is sensitive to the WP properties and/or the distance from WP to the water table. The initial free surface motions away from SGZ (~1 DOB or more) are not influenced by the latter two phases and may, therefore, be more reliable indicators of the yield of the device than are the SGZ motions (which are so sensitive to details of the geology). For a "HEARTS class" event, the peak energy associated with spall, and potentially available for the generation of (secondary) seismic waves, is about one-fourth the seismic energy available directly from the point source explosion.

The fact that the third pulse is associated with rebound has implications for underground test containment since rebound, and the resulting formation of a residual stress field, is central in the containment analysis of NTS underground tests. There is a potential for analyzing cavity growth and rebound from surface observations, a rather surprising and exciting possibility. We have not determined that unusually high free-surface velocities are "bad" for containment. More analyses of the calculations is required, but now that we better understand the underlying physical mechanisms that result in such high surface motions, we feel we are on firmer ground to make such analyses.

On Pahute Mesa, spallation appears to be less complicated than in Yucca Flat. For the two cases we have looked at, the mechanics of spall would appear to follow the standard treatments often employed in spall analyses. In general, the reflection from the free surface probably does not result in additional shear failure of the near surface materials so elastic superposition of stresses probably applies. We demonstrated calculationally that WP saturation and strength of the rocks out to a few cavity radii are primarily responsible for the observed differences in surface motions between TOWANDA and HOUSTON. This is not a particularly surprising result, but we are pleased that we can replicate this observation using rather straightforward modelling techniques. We have seen that a near surface, low impedance layer has a significant influence on the pattern of spall, although we currently lack the parameter studies to be more definitive on this. We could make the argument from the dynamics that such a near surface low velocity layer as exists at TOWANDA is somewhat analogous to a shallower SDOB. As is the case for the higher yield events in Yucca Flat, the energy associated with spall is about one-fourth that available for seismic waves from the point source explosion.

Table IV summarizes the energy partitioning for the cases covered in this paper.

Table IV

Energy Partitioning Summary

Event/ Case	Peak Energy in Spall (% of Total)	Peak Energy in Elastic Field (% of Total)	Ratio of Peak Spall/Elastic Energy
MERLIN Baseline	0.009	0.087	0.103
MERLIN Case A	0.021	0.151	0.139
MERLIN Case B	0.008	0.114	0.073
MERLIN Case C	0.008	0.140	0.061
HEARTS Baseline	0.085	0.320	0.266
HEARTS Case A	0.046	0.196	0.234
HEARTS Case B	0.063	0.359	0.176
HEARTS Case C	0.104	0.334	0.310
TOWANDA Baseline	0.159	0.595	0.267

V. ACKNOWLEDGMENTS

This work was performed under the auspices of the U. S. Department of Energy. Support for some of the work was provided by the DOE Office of Arms Control through the Los Alamos Source Region Program. The authors would like to thank Jack W. House, Nuclear Test Containment Program Manager for his continuing support of our work. Also, special thanks to Jake Perea, Bob Fitzhugh, Alex Salazar, George Chandler, Jim Turner and other members of the Los Alamos Field Instrumentation Group (J-8) for their high level of cooperation and positive efforts over the years in obtaining the ground motion data so vital to this investigation and others like it.

VI. REFERENCES

App, F. N., Brunish, W. M. and Edwards, C. L., "Modelling of the HEARTS Event", Proceedings of the Fifth Symposium on Containment of Underground Nuclear Explosions", CONF-8909163-Vol. 2, Mission Research Corporation, Santa Barbara, CA, 19-21 Sept. 1989.

App, F. N. and Brunish, W. M., "Stress Wave Calculations of Four Selected Underground Nuclear Tests: MERLIN, HEARTS, PRESIDIO and MISTY ECHO", Los Alamos Informal Report EES-NTS-91-03, Jan. 1991.

Brunish, W. M. and App, F. N., "Modelling of the MERLIN Event", Proceedings of the Fifth Symposium on Containment of Underground Nuclear Explosions", CONF-8909163-Vol. 2, Mission Research Corporation, Santa Barbara, CA, 19-21 Sept. 1989.

Brunish, W. M. and App, F. N., "Modelling and Comparison of Two Tunnel Events at the Nevada Test Site", Los Alamos National Laboratory Report - In Preparation, 1991.

Chilton, F., Eisler, J. D. and Heubach, H. G., "Dynamics of Spalling of the Earth's Surface Caused by Underground Explosions", J. Geophys. Res., 71,24,5911-5919, Dec. 1966.

Eisler, J. D. and Chilton, F., "Spalling of the Earth's Surface by Underground Nuclear Explosions", J. Geophys. Res., 69,24,5285-5293, Dec. 1964.

Eisler, J. D., Chilton, F. and Sauer, F. M., "Multiple Subsurface Spalling by Underground Nuclear Explosions", J. Geophys. Res., 71,16,3923-3927, Aug. 1966.

Glenn, H. D., "Spall Study in One Dimension", Lawrence Livermore National Laboratory Report UCID-17144, Apr. 1976.

Patton, H. J., "Characterization of Spall from Observed Strong Ground Motion on Pahute Mesa", Bull. Seis. Soc. Am., 80,5,1326-1345, Oct. 1990.

Perret, W. R., "Free Field and Surface Motion from a Nuclear Explosion in Alluvium: MERLIN Event", Sandia National Laboratory Report SC-RR-69-334, Nov. 1971.

Rinehart, J. S., "How to Predict the Effects of Spalling", Eng. and Min. J., 161,8,98-101, Aug. 1960.

Stump, B. W. and Weaver, T. A., "Physical Models of Spall Zone Ground Motions and the Determination of Spatial Decay Rates", Los Alamos National Laboratory Report - in Preparation, 1991.

Swegle, J. W., "TOODY IV - A Computer Program for Two-Dimensional Wave Propagation", Sandia National Laboratory Report SC-RR-66-2673, Mar. 1968.

END

DATE FILMED

11/01/93